

Surface Charge and Coating of CoFe₂O₄ Nanoparticles: Evidence of Preserved Magnetic and Electronic Properties

Silvia Nappini, Elena Magnano, Federica Bondino, Igor Piš, Alessandro Barla, Elvira Fantechi, Francesco Pineider, Claudio Sangregorio, Lisa Vaccari, Leonardo Venturelli, and Piero Baglioni

J. Phys. Chem. C, **Just Accepted Manuscript** • DOI: 10.1021/acs.jpcc.5b04910 • Publication Date (Web): 19 Oct 2015

Downloaded from <http://pubs.acs.org> on November 2, 2015

Just Accepted

“Just Accepted” manuscripts have been peer-reviewed and accepted for publication. They are posted online prior to technical editing, formatting for publication and author proofing. The American Chemical Society provides “Just Accepted” as a free service to the research community to expedite the dissemination of scientific material as soon as possible after acceptance. “Just Accepted” manuscripts appear in full in PDF format accompanied by an HTML abstract. “Just Accepted” manuscripts have been fully peer reviewed, but should not be considered the official version of record. They are accessible to all readers and citable by the Digital Object Identifier (DOI®). “Just Accepted” is an optional service offered to authors. Therefore, the “Just Accepted” Web site may not include all articles that will be published in the journal. After a manuscript is technically edited and formatted, it will be removed from the “Just Accepted” Web site and published as an ASAP article. Note that technical editing may introduce minor changes to the manuscript text and/or graphics which could affect content, and all legal disclaimers and ethical guidelines that apply to the journal pertain. ACS cannot be held responsible for errors or consequences arising from the use of information contained in these “Just Accepted” manuscripts.



1
2
3
4
5
6
7
8
9
10
11
12
13
14
15
16
17
18
19
20
21
22
23
24
25
26
27
28
29
30
31
32
33
34
35
36
37
38
39
40
41
42
43
44
45
46
47
48
49
50
51
52
53
54
55
56
57
58
59
60

Surface Charge and Coating of CoFe_2O_4 Nanoparticles: Evidence of Preserved Magnetic and Electronic Properties

Silvia Nappini,^{a} Elena Magnano,^a Federica Bondino,^a Igor Piš,^{a,b} Alessandro Barla,^c Elvira Fantechi,^d Francesco Pineider,^d Claudio Sangregorio,^e Lisa Vaccari,^b Leonardo Venturelli,^a and Piero Baglioni^f.*

^aIOM CNR, Laboratorio TASC, S.S. 14 km 163.5, 34149 Basovizza, Trieste, Italy

^bElettra-Sincrotrone Trieste S.C.p.A., S.S. 14 km 163.5, 34149 Basovizza, Trieste, Italy

^cIstituto di Struttura della Materia, ISM CNR, S.S. 14 km 163.5, 34149 Basovizza, Trieste, Italy

^dINSTM and Department of Chemistry, via della Lastruccia 3, 50019 Sesto F.no, Florence, Italy

^eINSTM and ICCOM CNR, Via Madonna del Piano 10, 50019 Sesto F.no, Florence, Italy

^fCSGI and Department of Chemistry, via della Lastruccia 3, 50019 Sesto F.no, Florence, Italy

KEYWORDS magnetic nanoparticles, hyperthermia, x-ray absorption spectroscopy (XAS), x-ray magnetic circular dichroism (XMCD), x-ray photoemission spectroscopy (XPS).

ABSTRACT

Magnetic nanoparticles (MNPs) have shown exceptional potential for several biological and clinical applications. However, MNPs must be coated by a biocompatible shell for such applications. The aim of this study is to understand if and how the surface charge and coating can affect the electronic and magnetic properties of CoFe_2O_4 MNPs. The role of the surface on the total magnetic moment of MNPs is a controversial issue, and several effects can contribute to make it deviate from the bulk value, including the charge, the nature of the coating but also the synthetic technique. Positively and negatively charged uncoated CoFe_2O_4 NPs, as well as citrate-coated NPs were prepared by soft chemistry synthesis. The electronic properties and cationic distribution of CoFe_2O_4 NPs were probed by X-ray Absorption Spectroscopy (XAS), X-ray Magnetic Circular Dichroism (XMCD) and X-ray Photoemission Spectroscopy (XPS) techniques, and confirmed by theoretical simulations. The overall magnetic behavior and the hyperthermic properties were evaluated by magnetometry and calorimetric measurements, respectively. The results show that all the investigated CoFe_2O_4 NPs have high magnetic anisotropy energy, and the surface charge and coating do not influence appreciably their electronic and magnetic properties. In addition, the citrate shell improves the stability of the NPs in aqueous environment, making CoFe_2O_4 NPs suitable for biomedical applications.

1. Introduction

Magnetic nanoparticles (MNPs) have risen great interest because of their remarkable magnetic, electric, physical and chemical properties, which, in most cases, are different from those of the bulk materials. Thanks to their intriguing properties, MNPs have found applicability in many

1
2
3 different areas, such as fabrication of electronic components for information storage, magnetic
4 cards, recording devices, catalysis¹⁻⁵, and, when properly functionalized, they represent a
5 promising approach for drug delivery, magnetic fluid hyperthermia (MFH), magnetic resonance
6 imaging (MRI), tissue engineering and bioanalysis⁶⁻¹². In particular, magnetic spinel ferrites
7 ($M_xFe_{3-x}O_4$, where M = Fe, Co, Ni, Mn or Zn) are emerging as innovative nanostructures for
8 many biological applications, where a superparamagnetic behaviour, a high magnetization value,
9 a diameter smaller than a critical value (typically around 10-20 nm), a narrow size distribution
10 and an appropriate surface coating are required. Among magnetic spinel ferrite NPs, $CoFe_2O_4$
11 has received a lot of attention for its unique magnetic properties, such as a large anisotropy
12 energy, tuneable coercivity and high saturation magnetization, that make $CoFe_2O_4$ NPs good
13 candidates to be used for MRI and MFH^{10,11}.

14
15 For applications, such as MRI, MFH and drug delivery, the ability to control magnetic
16 anisotropy, together with the possibility of controlling NP size and surface composition could
17 provide a method to optimize the NP relaxation time for a specific applied field frequency. Large
18 heating effects are essential to realize magnetic-based therapeutic treatments; however, a
19 biocompatible coating to prevent NP aggregation without affecting the magnetic properties is
20 essential for biomedical applications of $CoFe_2O_4$ NPs.

21
22 Most of mixed ferrites, such as $CoFe_2O_4$, exhibit partially inverted spinel structure. At the
23 nanoscale level, the inversion degree, corresponding to the fraction of divalent ions in octahedral
24 (O_h) sites, can significantly depend on synthesis conditions, especially on the Co/Fe ratio in the
25 precursor solution and the reaction temperature¹³⁻¹⁵. The replacement of Fe^{2+} cations with the
26 more anisotropic Co^{2+} cations allows an increase in the magneto-crystalline anisotropy up to 20
27 times in comparison with that of magnetite.

1
2
3 The magnetic properties of ferrites depend on many factors, including the composition, the
4 cation distribution into the crystallographic structure, the shape, the size, and the surface
5 morphology^{16,17}.
6
7

8
9
10 The shape and the size of NPs can significantly affect the total magnetic anisotropy of the
11 material. In the absence of an applied magnetic field, a magnetically isotropic material has no
12 preferential direction for its magnetic moment, while a magnetically anisotropic material will
13 align its moment with one of the easy axes. In fact, when a particle is not perfectly spherical, the
14 demagnetizing field will not be equal for all directions. Moreover for decreasing diameters, the
15 surface area becomes larger with respect to the bulk, and thus more cations are located close to
16 it, resulting in a greater disordered distribution of the electron spins on the surface because of
17 their reduced spin-spin exchange^{17,18}.
18
19

20 The alteration of the surface morphology is another parameter that might change the cation
21 distributions and consequently the magnetic properties of NPs.
22
23

24 Generally, several surface factors can contribute to change the surface morphology and to
25 deviate the total magnetic moment of nanometric particles from the bulk value, including the
26 number and type of defects, vacancies, inversion degree and surface disorder. All these
27 parameters strongly depend by the nature of the coating but also by the synthetic technique
28 adopted to prepare NPs.
29
30

31 The surface coating is fundamental for biomedical applications, and can regulate the physical
32 and chemical stability of the system, preventing NP aggregation in physiological environment,
33 and providing also a higher biocompatibility. The NP coating is generally obtained by chemical
34 functionalization with organic or inorganic ligands, polymers, surfactants, dextran and
35 phospholipids¹⁹⁻²³. The nature of the surface shell can affect the water accessibility to the
36
37
38
39
40
41
42
43
44
45
46
47
48
49
50
51
52
53
54
55
56
57
58
59
60

1
2
3 magnetic core, influencing also the magnetic properties and relaxivity of the MNPs. Despite
4 several studies on the structural characterization of CoFe_2O_4 NPs have already been done, little is
5 reported on their electronic and magnetic properties as a function of different surface
6 functionalization. However, a deeper understanding of the electronic, magnetic, chemical and
7 physical properties of CoFe_2O_4 NPs is fundamental for their applicability in different fields of
8 research.
9

10
11 In this paper, we report a detailed investigation on the structure, oxidation state, electronic and
12 magnetic properties of CoFe_2O_4 NPs with three different types of stabilization: positively and
13 negatively charged uncoated NPs, and citrate coated NPs. These types of NPs are stable and well
14 dispersed in aqueous solution because of the electrostatic and steric repulsion achieved by
15 surrounding NPs with ionic species and a capping agent (citric acid). Citrate coating is widely
16 used to obtain stable NPs in physiological solution thanks to the presence of terminal water-
17 exposed carboxylate groups, which also provide good anchoring sites for further surface
18 functionalization (i.e. with fluorescent dyes or molecules of biomedical interest).
19

20
21 All the investigated samples were obtained by soft chemistry synthesis, as reported in detail in
22 the experimental section. The size, shape and morphology of the NPs were investigated by
23 means of small angle X-ray scattering (SAXS) and transmission electron microscopy (TEM)
24 measurements and the composition and the citrate coordination were determined by Inductively
25 Coupled Plasma–Atomic Emission (ICP-AES) and Attenuated Total Reflectance Fourier-
26 Transform Infrared (ATR-FTIR) spectroscopy.
27

28
29 Information on the chemical states of Co and Fe cations, the effect of different surface charges,
30 as well as the chemical bonding of the citrate shell were obtained by X-ray photoemission
31 spectroscopy (XPS). A detailed analysis of the electronic properties, including the oxidation
32
33
34
35
36
37
38
39
40
41
42
43
44
45
46
47
48
49
50
51
52
53
54
55
56
57
58
59
60

1
2
3 state, and distributions of Co and Fe cations over the T_d and Oh sites was performed by Soft X-
4 ray Absorption Spectroscopy (XAS) and X-ray magnetic circular dichroism (XMCD) methods.
5
6

7
8 The overall magnetic behavior of both uncoated and citrate-coated CoFe_2O_4 NPs was
9 evaluated by collecting hysteresis curves at 2.5 K with a vibrating sample magnetometer (VSM).
10
11

12 Calorimetric experiments were also performed on all the MNP samples to evaluate their
13 Specific Absorption Rate (SAR), that is proportional to the MNP capability to release heat upon
14 an alternating magnetic field (AMF). The SAR is an important parameter for MFH, which
15 represents one of the most promising clinical applications of MNPs based on the destruction of
16 tumor cells through the heat released from the particles upon an AMF.
17
18
19
20
21
22
23
24
25
26

27 2. Experimental Methods

28
29 **Cobalt Ferrite Nanoparticle Synthesis.** CoFe_2O_4 NPs were prepared according to the method
30 developed by Massart²⁴, introducing minor modifications as previously reported^{6,7,25}. Solutions
31 of 1 M FeCl_3 (64 ml) and $\text{Co}(\text{NO}_3)_2$ (32 ml) were added to concentrated nitric acid (2 ml). The
32 mixture was heated to boiling point and then mixed under vigorous agitation with a boiling
33 solution of NaOH 1M (400 ml). The boiling temperature (100 °C) and the stirring were
34 maintained for 90 minutes. The obtained NPs were separated by magnetic decantation, washed
35 with water and re-suspended in 40 ML of HNO_3 2M. After a second magnetic decantation, the
36 NPs were dispersed in a boiling solution of 0.5 M FeCl_3 (56 ml) and 0.5 M $\text{Co}(\text{NO}_3)_2$ (28 ml) and
37 kept under vigorous agitation for 30 minutes. The precipitate was isolated, washed with water
38 and dispersed in 0.25 M TMAH (tetramethylammonium hydroxide solution), obtaining
39 negatively charged CoFe_2O_4 NPs. Positively charged CoFe_2O_4 NPs were obtained by washing
40 the precipitate with HNO_3 1 M (30 ml) and dispersing it in water
41
42
43
44
45
46
47
48
49
50
51
52
53
54
55
56
57
58
59
60

1
2
3 Citrate-coated cobalt ferrite NPs were prepared starting from the uncoated NPs dispersed in
4 TMAH by coordination of citric acid. Uncoated MNPs (10 ml, 1% wt) were added to a 100 mM
5 citric acid solution (30 ml) and slightly stirred for 1 h at room temperature (the resulting pH was
6 around 5). After recollecting the precipitate with the magnet, NPs were dispersed in 20 mM tri-
7 sodium citrate (30 ml) and kept under stirring for 45 min. The obtained particles were separated
8 by magnetic decantation and washed several times with water and acetone in order to remove
9 any excess of citric acid. The citrate coated MNPs were gently dried under a nitrogen gas flux,
10 dispersed in the buffer solution (10 mM HEPES, 107 mM NaCl, 5.3 mM NaOH, pH 7.4) and
11 kept under slight stirring for 24 h. The dispersion was finally centrifuged at 1000 g for 2 min and
12 the supernatant was dialyzed against water for 24 h through a cellulose dialysis bag (avg. flat
13 width 23 mm, MWCO 12400, 99.99% retention) in order to remove non-coordinated citrate
14 species. A residual ionic strength is, however, always present because of solvated anions in
15 equilibrium with the adsorbed ones. The citrate coordination of the metals on CoFe_2O_4 NP
16 surface was verified by ATR-FTIR spectroscopy.
17
18
19
20
21
22
23
24
25
26
27
28
29
30
31
32
33
34
35

36 **X-ray Absorption (XAS), X-ray Magnetic Circular Dichroism (XMCD) and X-ray**
37 **Photoemission Spectroscopy (XPS).** XAS, XMCD and XPS measurements were carried out at
38 the BACH beamline (Beamline for Advanced diChroism) at Elettra synchrotron facility in
39 Trieste (Italy). Due to the limitation of XAS, XMCD and XPS to UHV conditions, samples were
40 dried prior to the measurements. Specifically, samples were prepared by dropcast method, where
41 a drop of CoFe_2O_4 NPs suspension was deposited onto a clean Si wafer and left to dry. The
42 experimental data were collected under UHV conditions (base pressure $\geq 1 \times 10^{-10}$ mbar) and with
43 a photon flux of 10^{12} photons/s.
44
45
46
47
48
49
50
51
52
53
54
55
56
57
58
59
60

1
2
3 XAS spectra at the $L_{3,2}$ edges of Fe and Co, and K edge of O were measured both in total
4 electron yield (TEY) mode and in total fluorescence yield (TFY) mode, ensuring either surface
5 or bulk sensitivities, respectively. TEY spectra were recorded by measuring the drain current
6 with an energy resolution better than 0.1 eV, TFY spectra were recorded using a silicon
7 photodiode with an energy resolution better than 0.16 eV.

8
9
10 XMCD measurements in high a magnetic field (up to 3 T) along the beam direction at a
11 temperature of 11 K and 150 K were carried out on negative uncoated CoFe_2O_4 NPs. The
12 polarization of the incident light was flipped between the positive (σ^+) and negative (σ^-) photon
13 helicity and the spectra were recorded in TEY mode.

14
15 XPS angle integrated spectra of Fe 2p and Co 2p, as well as O 1s core levels were collected at
16 RT using a hemispherical electron energy analyzer Scienta R3000, with a total energy resolution
17 of 130 meV, in normal emission geometry, with an angle of 60° between the incident light and
18 the normal to the surface. Co 2p and Fe 2p spectra were measured at a photon energy of 1099
19 eV, while O 1s spectrum was measured at a photon energy of 734 eV. The O 1s spectra were
20 fitted using Voigt functions and Shirley type background²⁶.

21
22 The XAS and XMCD signals were simulated by Ligand Field Multiplet (LFM) calculation and
23 compared to the experimental XAS spectra in order to elucidate the origin of the different
24 spectral features. The LFM model calculates the spectra of each cation in a given crystal field
25 (octahedral or tetrahedral symmetry), giving the oxidation state and quantitative information
26 about the site occupancy of each ion state. LFM simulations were carried out using the
27 CTM4XAS 5.5 program including full spin-orbit coupling, crystal field effects, and the reduction
28 of the Slater integrals $F(dd)$, $F(pd)$ and $G(pd)$ to consider the electronic repulsions²⁷.

29
30
31
32
33
34
35
36
37
38
39
40
41
42
43
44
45
46
47
48
49
50
51
52
53
54
55
56
57
58
59
60

1
2
3 **Inductively Coupled Plasma–Atomic Emission Spectrometry (ICP-AES).** A VARIAN 720
4
5 OES inductively coupled plasma optical emission spectrometer (ICP-AES) was used for the
6
7 determination of iron and cobalt content (ppm) of CoFe_2O_4 NP dispersions. The samples were
8
9 diluted from 0.1 ml to 5.0 ml in 0.1% nitric acid. Calibration curves of standard solutions of iron
10
11 and cobalt were used. The ICP-AES was programmed to detect Co (238.892; 228.615; 230.786
12
13 nm) and Fe (238.204; 259.940; 234.350 nm) and to give the average value of the obtained results
14
15 for each metal. An internal standard of Ge 5 ppm (209.426 nm) was used to correct for matrix
16
17 effects.
18
19
20
21

22 **Transmission Electron Microscopy (TEM).** TEM investigations were carried out using a
23
24 Philips CM 12 electron microscope operating at acceleration voltages up to 120 kV and equipped
25
26 with an Olympus MegaViewG2 side-mounted CCD camera. Samples were prepared by placing
27
28 drops of the suspensions on a carbon-coated copper grid with a carbon membrane film and
29
30 removing the excess solvent with filter paper.
31
32
33

34 **Attenuated Total Reflection Infrared Spectroscopy (ATR-FTIR).** FTIR spectra were
35
36 collected using a VERTEX 70 interferometer (Bruker) purged with nitrogen and DTGS
37
38 (deuterated tri glycine sulfate) detector. MIRacle Single Reflection ATR box (PIKE
39
40 Technologies) equipped with a diamond IRE (Internal Reflection Element) was chosen for the
41
42 purpose of the experiment. Five microliters of citrate coated CoF_2O_4 NPs dispersed in water
43
44 were dropped onto the crystal and the measurements were repeated until vanishing of the
45
46 combination band of bending and vibrational modes of liquid water, centered at $\sim 2150 \text{ cm}^{-1}$.
47
48 The background was collected on the clean IRE element. Spectra were acquired averaging 128
49
50 scans with a spectral resolution of 4 cm^{-1} .
51
52
53
54
55
56
57
58
59
60

1
2
3 **Small Angle X-Rays Scattering (SAXS).** SAXS measurements were carried out with a
4 HECUS SWAX-camera (Kratky) equipped with a position-sensitive detector (OED 50 M)
5 containing 1024 channels of the width of 54 μm . Cu K_{α} radiation of wavelength 1.542 \AA was
6 obtained using an X-ray generator (Seifert ID-3003) operating at a maximum power of 2 kW. A
7 10 μm thick nickel filter was used to remove Cu K_{α} radiation. The volume between the sample
8 and the detector was kept under vacuum (pressure less than 1 mBar) during measurements to
9 minimize scattering from air. The liquid samples were filled into 1 mm quartz capillary and then
10 sealed. Measurements were done at 25 $^{\circ}\text{C}$ and the temperature was controlled by a Peltier
11 element, with an accuracy of ± 0.1 $^{\circ}\text{C}$. All scattering curves were corrected for the solvent
12 contribution. The data were slit desmeared by a linear method²⁸.
13
14
15
16
17
18
19
20
21
22
23
24
25
26

27 **Magnetometry.** Magnetic measurements were performed with a PPMS VSM magnetometer
28 (Quantum Design, San Diego, USA) mounting a liquid helium cryostat and a superconducting
29 coil magnet. The magnetization curves were recorded at 2.5 K and the data were corrected for
30 the diamagnetic contribution of the sample holder which was measured separately.
31
32
33
34
35
36

37 **Hyperthermic characterization.** The hyperthermic properties of the CoFe_2O_4 NPs samples,
38 were investigated by recording temperature kinetics during the exposition to an AMF. The
39 experimental set-up was composed by a 6 kW Fives Celes® power supply, a water-cooled
40 induction coil and a series of capacitors. The field parameters (183 kHz, 17.0 kA/m) were chosen
41 in order to operate within the physiological limit, $H \nu < 5 \cdot 10^9 \text{Am}^{-1} \text{s}^{-1}$, beyond which deleterious
42 responses of living tissues were observed²⁹. Samples were placed in the middle of the induction
43 coil, hosted in a polystyrene sample holder inside a glass container thermostated by a flow of
44 ethylene glycol. The temperature of the samples, recorded by an optical fiber thermometer
45 dipped into the sample, was allowed to stabilize to 25 $^{\circ}\text{C}$ prior to the measurement. The
46
47
48
49
50
51
52
53
54
55
56
57
58
59
60

1
2
3 concentration of CoFe_2O_4 in the measured samples was 0.56% w/w for negative, 0.64% w/w for
4
5 positive and 0.51% w/w for citrate. The Specific Absorption Rate(SAR) value, i.e. the power
6
7 dissipated by the material as a function of the unit mass, was evaluated using the formula
8
9

$$10 \quad SAR = \frac{c_{H_2O} m_{H_2O} \Delta T}{m_{Me} \Delta t}$$

11
12
13
14
15 Where m_{Me} is the total mass of metals (Fe and Co), c_{H_2O} and m_{H_2O} the specific heat and mass of
16
17 water, respectively. ΔT is the temperature increase in the interval of time Δt . Since the
18
19 measurements are carried in non-adiabatic conditions, the $\Delta T/\Delta t$ value was extrapolated by
20
21 taking the initial slope of the temperature kinetic curve.
22
23
24
25
26
27

28 **3. Results and discussion**

29
30
31 **Structural and electronic characterization.** Three types of CoFe_2O_4 NP samples (negatively,
32
33 positively charged uncoated, and citrate coated MNPs) were prepared according to the Massart
34
35 method (see Experimental Methods) and then functionalized with citric acid to obtain the citrate
36
37 coated ones. All the samples are well dispersible in aqueous solution: the citrate coated NPs are
38
39 particularly stable under physiological conditions thanks to the shell of citrate anions, while the
40
41 alkaline ones are chemically stabilized by TMAH, that acts as a surfactant and peptizing agent
42
43 creating an electrostatic repulsion layer surrounding the particles. Similarly, in the case of acidic
44
45 NPs, the electrostatic repulsion is achieved by protonation of the NP surface, through addition of
46
47 HNO_3 to the alkaline dispersion.
48
49
50
51

52 A schematic picture of the stabilization of the investigated MNPs is depicted in Figure 1,
53
54 where the possibility to obtain stable nanoparticles in aqueous solution by adding a surfactant
55
56 (TMAH or HNO_3) or a capping agent (citric acid) is displayed.
57
58
59
60

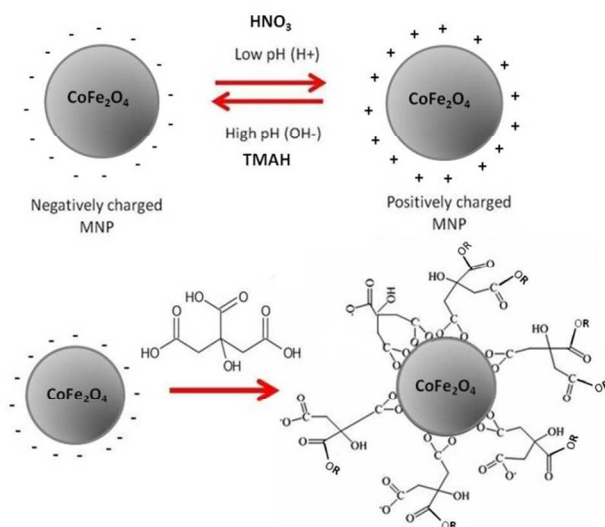


Figure 1. Scheme of the mechanism of stabilization of negatively, positively and citrate coated CoFe₂O₄ NPs. Stable MNPs in solution are obtained by using suitable surfactants such as TMAH for negatively charged NPs and HNO₃ for positively charged NPs. The double arrows indicate the possibility to shift from negative to positive NPs (and viceversa) by adding the corresponding agents (therefore changing the pH of the solution and the surface charge of NPs). Citrate coated MNPs are obtained by coordination of negatively coated NPs with a capping agent (citric acid) added to the solution.

The size, shape and morphology of uncoated and citrate-coated cobalt CoFe₂O₄ NPs were described and characterized in detail by means of TEM and SAXS.

TEM pictures and the corresponding size distributions are reported in Figure 2, which shows that all the three NP samples are quite mono-disperse with a nearly spherical shape and an average diameter of 7 ± 3 nm. It is important to point out that the citrate coating cannot be detected by TEM because of its low electronic density and small thickness (less than 1 nm). Generally TEM is restricted to small volumes and hence to low precipitate populations, making it poorly suited for statistical analysis³⁰.

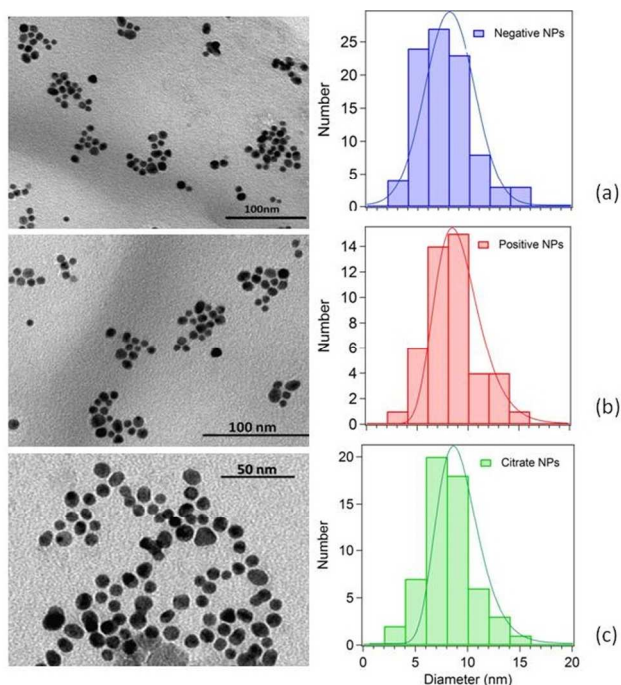


Figure 2. TEM images and the corresponding size distribution of (a) negatively charged uncoated, (b) positively charged uncoated and (c) citrate coated CoFe_2O_4 NPs .

In order to have information about the average diameter and the size distribution in aqueous solution, SAXS measurements were performed directly on the NPs dispersed in water. In comparison to TEM, SAXS benefits from higher statistical quality in the size distribution determination within one measurement and presents no limitation imposed by drying the sample, which can lead to aggregation or other physical change³⁰.

SAXS analysis of uncoated and citrate coated CoFe_2O_4 NPs were well described in previous works^{6,7}, where the spectra were modelled according to the formalism introduced by Bartlett and Ottewill for polydisperse spherical particles³¹, considering the particles as spherical objects with a Schulz distribution of radii^{32,33}. No structure factors were included in this model because of the low concentration of particles in the dispersions, so that inter-particle interference effects can be neglected. The fitting results summarized in Table 1 show that the obtained radii of uncoated and

1
2
3 citrate-coated NPs are very similar because the electron density in CoFe_2O_4 NPs largely
4
5 overrules that of the citrate shell, resulting in a SAXS signal that accounts only for the metal
6
7 oxide cores.
8
9

10 The slight difference in the size of the NPs determined from SAXS as compared to TEM is
11
12 mainly due to the fact that the statistical analysis of the particle distribution from TEM images
13
14 was done considering only small regions, where aggregates were not present because
15
16 deliberately omitted from the measurements, while SAXS analysis was done in solution
17
18 providing an average value of the NP size.
19
20
21
22
23

24 **Table 1.** Structural parameters of CoFe_2O_4 NPs dispersed in water obtained by SAXS. $\langle D \rangle$
25
26 stands for mean diameter.
27
28
29

	Citrate coated CoFe_2O_4	Uncoated $\text{CoFe}_2\text{O}_4(-)$	Uncoated $\text{CoFe}_2\text{O}_4(+)$
<i>SAXS Fitting</i>			
$\langle D \rangle$ [nm]	9.8 ± 0.2	11.2 ± 0.4	11.8 ± 0.4
Polydispersity	0.60 ± 0.01	0.49 ± 0.02	0.42 ± 0.01

30
31
32
33
34
35
36
37
38
39
40
41
42 Iron and Cobalt content in the three CoFe_2O_4 NP samples was checked by ICP-AES indicating
43
44 a ratio Fe/Co around 2.12, very close to the expected ratio of 2. The concentration of the "as
45
46 prepared" samples (mother solutions) are reported in the S.I., and eventually decreased by
47
48 dilution for the experiments.
49

50
51 The surface functionalization of CoFe_2O_4 NPs with citrate was proved by ATR-FTIR
52
53 measurements by comparing the NP spectrum with citric acid (ligand precursor) and tri-sodium
54
55 citrate (reference) spectra to understand the mechanism of citrate coordination to NPs.
56
57
58
59
60

A comparison among the ATR-FTIR³⁴ spectra of citrate coated CoFe₂O₄ NPs (70 mM), tri-sodium citrate (20 mM) and citric acid (20 mM) aqueous solutions is shown in Figure 3 and the results are summarized in Table 2.

The intense peak centred at 1709 cm⁻¹ in the spectrum of pure citric acid can be assigned to the carbonyl stretching of the carboxylic group (COOH). This contribution is totally suppressed in the spectrum of the pure tri-sodium citrate, characterized by two strong bands centred at 1572 and 1390 cm⁻¹, respectively assignable to asymmetric and symmetric stretching of carbonyl group of free-carboxylate anion (COO⁻), and by a broad band centred at 1255 cm⁻¹, related to the combination of stretches and bends of carboxylate group³⁵.

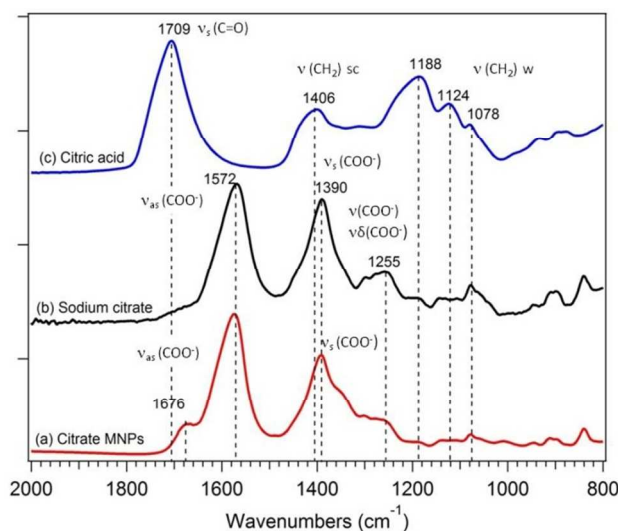


Figure 3. ATR-FTIR spectra of (a) citrate coated CoFe₂O₄ NPs at pH=7.4, (b) 20 mM trisodium citrate solution, and (c) 20 mM citric acid solution.

In addition to those peaks, the ATR-FTIR spectrum of citrate-coated NPs shows a band centred at 1676 cm⁻¹, that clearly indicates that citric acid binds to NP surface through coordination of the carboxylate functionalities of citrate anions, as already reported^{36–39}. Indeed, carboxylic groups of citric acid chemisorbed onto the NP surface possess a partial single bond

character that results in the weakening of the C=O bond and determines the shift to lower frequency of the stretching of the C=O group coordinated onto the surface of CoFe₂O₄. It is therefore possible to envision that citric acid forms complexes with the metal cations of CoFe₂O₄ by chemisorption of one or two of the three COO⁻ functionalities, depending on steric and curvature of the surface, while the residual carboxylate groups do not interact with NP^{37,39}, and therefore preserve characteristics of free carboxylate moieties. This coordination scheme is further supported by the more pronounced asymmetry of the symmetric stretching of COO⁻ moieties, that indicates the presence of at least two types of $\sim\nu_{\text{sym}}(\text{COO}^-)$.

Table 2. FTIR vibrational assignments at citric acid, tri-sodium citrate and citrate coated CoFe₂O₄ NPs.

Vibrational modes	Frequency (cm ⁻¹)		
	Citric acid	Trisodium citrate	Citrate-coated NPs
ν_s (C=O, COOH)	1709	—	1676 (chemisorbed)
ν_{as} (COO ⁻)	—	1572	1572 (free)
ν_s (COO ⁻)	—	1390	1390
ν (CH ₂)	1406(sc)/1078(w)	Convolved with ν_s (COO ⁻) /1078(w)	Convolved with ν_s (COO ⁻) /1078(w)
Combination of ν (COO ⁻) and δ (COO ⁻)	—	1300-1250	1300-1250

ν : stretching, δ : bending, sc: scissor, w: wagging, as: asymmetric, s: symmetric

According to the proposed coordination scheme, at least one carboxylate group results exposed to the solvent, and this group should be responsible for making the surface charged and hydrophilic.⁴⁰

1
2
3 In order to determine the cationic distribution in CoFe_2O_4 NPs and the effects of the citrate
4 coating and surface charge on the electronic properties of the three investigated MNP samples,
5 XAS, XMCD and XPS measurements were carried out.
6
7

8
9
10 Iron and cobalt $L_{3,2}$ edge XAS was used to estimate the oxidation state of Co and Fe in
11 CoFe_2O_4 NPs. The XAS spectra of the three samples were recorded both in TEY (surface
12 sensitive) and TFY (bulk sensitive) mode to investigate the level of uniformity of the chemical
13 composition. The total integrated intensity of each spectrum was normalized with respect to the
14 L_3 edge to show the relative changes between peak heights.
15
16
17
18
19
20
21

22 Fe $L_{3,2}$ and Co $L_{3,2}$ spectra ($2p \rightarrow 3d$) recorded in TEY for all three CoFe_2O_4 NP samples are
23 shown in Figure 4(a,b). TEY spectra clearly indicate that the NP surface has the typical structure
24 of iron oxides, where the octahedral crystal field lifts the degeneracy of both the $2p_{3/2}$ (L_3 edge)
25 and $2p_{1/2}$ (L_2 edge) levels of Fe, generating levels with t_{2g} and e_g symmetry^{41–43}. Iron L_3 edge
26 shown in Figure 4(a) consists of a main peak at 708.9 eV with a shoulder at 707.4 eV. The L_2
27 edge, which is separated from the L_3 edge by an energy corresponding to the spin-orbit splitting
28 of 2p core levels, also consists of two peaks (720.8 and 722.4 eV).
29
30
31
32
33
34
35
36
37
38
39
40
41
42
43
44
45
46
47
48
49
50
51
52
53
54
55
56
57
58
59
60

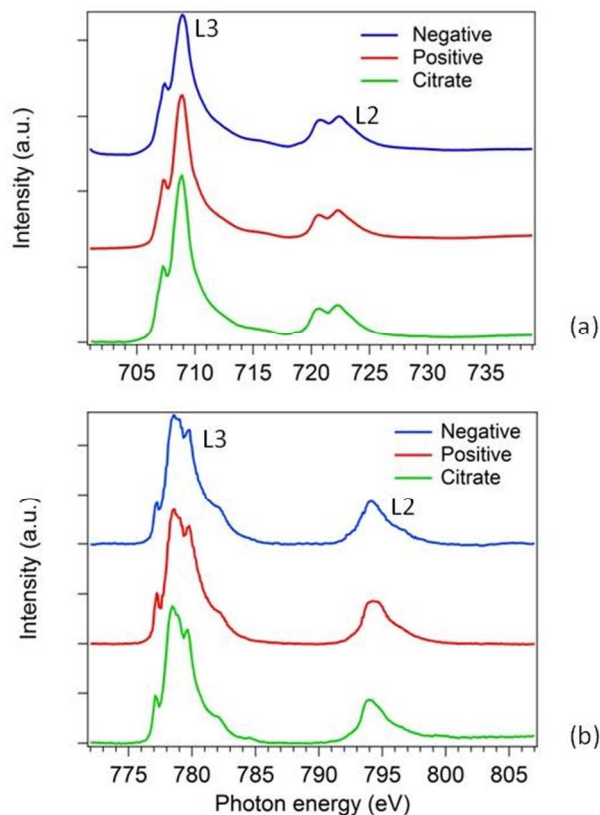


Figure 4. XAS spectra of (a) Fe L_{3,2} edge and (b) Co L_{3,2} edge of negatively and positively charged uncoated, and citrate coated CoFe₂O₄ NPs recorded in TEY mode.

The absence of detectable differences between the surface-sensitive TEY spectra of uncoated and citrate coated NPs indicates that the oxidation state of Fe cations on the surface is not affected by the presence of the citrate shell and the bulk sensitivity of TFY XAS (not shown) evidences that the bulk electronic structure of the CoFe₂O₄ NPs is the same as that of the surface.

The corresponding Co L_{3,2} spectra (2p→3d), recorded in TEY, are displayed in Figure 4(b). They exhibit the typical multiplet structure of octahedral Co²⁺ compounds.^{42–44}, where the L₃ edge is characterized by three peaks at 777.1, 778.5 and 779.7 eV, and by a shoulder at 782 eV, and the L₂ edge is around 794 eV.

1
2
3 Again, no differences were detected between citrate coated and uncoated CoFe_2O_4 NPs,
4 showing that the uppermost layer of Co ions is not affected by the citrate shell.
5
6

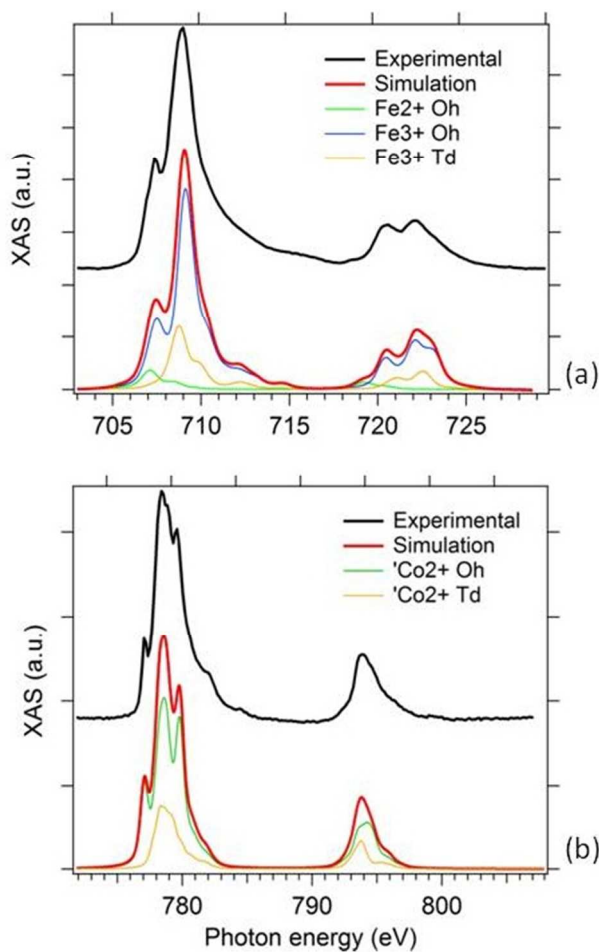
7
8 The experimental XAS spectra of Fe $L_{3,2}$ and Co $L_{3,2}$ were compared to those calculated using
9 the LFM model to assign the corresponding cationic contribution to each spectral feature (see
10 experimental section). The simulated spectra were obtained from a weighted superposition of the
11 individual spectra of each cationic species in the sample calculated considering a given crystal
12 field. The simulation defines which cation state is responsible for each peak, and provides the
13 site occupancies of each type of cations.
14
15
16
17
18
19
20
21

22 In the calculations, the Slater integrals $F(dd)$, $F(pd)$, and $G(pd)$ were reduced to 80%^{42,43,45} to
23 account for overestimation of the electron repulsion in solid compounds, and all the spectra were
24 broadened by a Lorentzian with a half-width of 0.2(0.3) eV and by a Gaussian with a half-width
25 of 0.2 eV^{42,46,47}.
26
27
28
29
30

31 Figure 5(a) shows the Fe $L_{3,2}$ XAS spectrum measured at the citrate-coated CoFe_2O_4 NPs
32 together with the simulated one obtained from the linear combination of the LFM calculated
33 spectra of Fe^{2+} octahedral (Oh), Fe^{3+} octahedral (Oh), and Fe^{3+} tetrahedral (Td) cations. The
34 crystal-field strengths (10Dq) were set to 1.5 for Oh cations, and 0.55 for Td cations, in
35 accordance with previous studies on similar ferrites^{42,46,47}. The best combination of individual
36 cationic spectra indicates that most of the Fe^{3+} ions are localized mainly at the Oh sites (71%),
37 while the other Fe^{3+} cations are located at the Td sites (19%). Surprisingly also some Fe^{2+}
38 species are present at the remaining Oh sites (10%), experimentally confirmed by the presence of
39 a small feature at 719.5 eV, that is generally considered a clear signature of octahedrally
40 coordinated Fe^{2+} ions⁴². In fact, Moyer et al. have shown that, in $\text{Co}_{(1-x)}\text{Fe}_{(2+x)}\text{O}_4$ thin film, a
41 small spectral shoulder at the lower energy side of the L_3 peak in Fe XAS spectra grows when
42
43
44
45
46
47
48
49
50
51
52
53
54
55
56
57
58
59
60

1
2
3 the concentration of Co is decreasing. This indicates that, as x increases, Fe is added to the
4 sample in the form of Fe^{2+} octahedral cations, replacing the Co^{2+} ions at the Oh sites.^{42,48}

5
6
7
8 Possible explanations about the unexpected presence of small amount of Fe^{2+} ions in CoFe_2O_4
9 NPs are provided later in the text.
10
11



45
46
47
48
49
50
51
52
53
54
55
56
57
58
59
60

Figure 5. Comparison between the calculated LFM spectra (red curves) and the experimental XAS spectra (black curves) of Fe $L_{3,2}$ edge (a) and Co $L_{3,2}$ edge (b) of CoFe_2O_4 NPs. The calculated spectral components corresponding to Fe^{3+} Oh, Fe^{3+} Td and Fe^{2+} Oh cations, and Co^{2+} Oh and Co^{2+} Td cations, respectively, are displayed as well.

1
2
3 The theoretical results for Co $L_{3,2}$ spectrum are displayed in Figure 5(b), where the individual
4 calculated contributions of Co^{2+} octahedral (Oh) and Co^{2+} tetrahedral (Td) cations, and the
5 experimental spectrum of $CoFe_2O_4$ NPs are shown as well. In this case, the crystal field strength
6 used for Co cations is 1.2 for Oh sites and 0.55 for Td sites, in accordance with previous
7 studies⁴². The Co^{2+} Oh cations give the strongest contributions (around 75%) , affecting the
8 three main features of L_3 in the experimental spectrum. The remaining 25% of Co^{2+} Td cations
9 contribute to the formation of the small shoulder at 782 eV.

10
11
12
13
14
15
16
17
18
19
20 The site occupancies of each type of cations is in accordance with previous studies^{44,49,50} ,
21 suggesting that Co cations are exclusively divalent, while Fe consists of a predominating
22 population of trivalent cations together with a small population of some divalent ions, even if the
23 ratio of Co to Fe was expected 1:2. These results suggest that during the $CoFe_2O_4$ NPs' synthesis
24 a deficiency of Co^{2+} ions is replaced by Fe^{2+} cations at Oh sites, preserving the overall neutral
25 charge balance of the unit cell. This hypothesis is also confirmed by ICP-AES measurements,
26 which showed a slightly predominance of Fe, indicating a ratio of Fe/Co equal to 2.12.
27 Nevertheless, part of the Co^{2+} can substitute also into the Fe^{3+} Td sites, but this implies an overall
28 negatively charged unit cell. Alternatively, part of the cobalt could substitute as Co^{3+} cations into
29 the Fe^{3+} Td sites, preserving in this way the charge balance⁵¹. However, the simulation of CoL_{32}
30 XAS spectra do not match very well with the experimental data when Co^{3+} Oh component is
31 introduced (data not shown).

32
33
34
35
36
37
38
39
40
41
42
43
44
45
46
47
48
49
50
51
52
53
54
55
56
57
58
59
60
61
62
63
64
65
66
67
68
69
70
71
72
73
74
75
76
77
78
79
80
81
82
83
84
85
86
87
88
89
90
91
92
93
94
95
96
97
98
99
100
101
102
103
104
105
106
107
108
109
110
111
112
113
114
115
116
117
118
119
120
121
122
123
124
125
126
127
128
129
130
131
132
133
134
135
136
137
138
139
140
141
142
143
144
145
146
147
148
149
150
151
152
153
154
155
156
157
158
159
160
161
162
163
164
165
166
167
168
169
170
171
172
173
174
175
176
177
178
179
180
181
182
183
184
185
186
187
188
189
190
191
192
193
194
195
196
197
198
199
200
201
202
203
204
205
206
207
208
209
210
211
212
213
214
215
216
217
218
219
220
221
222
223
224
225
226
227
228
229
230
231
232
233
234
235
236
237
238
239
240
241
242
243
244
245
246
247
248
249
250
251
252
253
254
255
256
257
258
259
260
261
262
263
264
265
266
267
268
269
270
271
272
273
274
275
276
277
278
279
280
281
282
283
284
285
286
287
288
289
290
291
292
293
294
295
296
297
298
299
300
301
302
303
304
305
306
307
308
309
310
311
312
313
314
315
316
317
318
319
320
321
322
323
324
325
326
327
328
329
330
331
332
333
334
335
336
337
338
339
340
341
342
343
344
345
346
347
348
349
350
351
352
353
354
355
356
357
358
359
360
361
362
363
364
365
366
367
368
369
370
371
372
373
374
375
376
377
378
379
380
381
382
383
384
385
386
387
388
389
390
391
392
393
394
395
396
397
398
399
400
401
402
403
404
405
406
407
408
409
410
411
412
413
414
415
416
417
418
419
420
421
422
423
424
425
426
427
428
429
430
431
432
433
434
435
436
437
438
439
440
441
442
443
444
445
446
447
448
449
450
451
452
453
454
455
456
457
458
459
460
461
462
463
464
465
466
467
468
469
470
471
472
473
474
475
476
477
478
479
480
481
482
483
484
485
486
487
488
489
490
491
492
493
494
495
496
497
498
499
500
501
502
503
504
505
506
507
508
509
510
511
512
513
514
515
516
517
518
519
520
521
522
523
524
525
526
527
528
529
530
531
532
533
534
535
536
537
538
539
540
541
542
543
544
545
546
547
548
549
550
551
552
553
554
555
556
557
558
559
560
561
562
563
564
565
566
567
568
569
570
571
572
573
574
575
576
577
578
579
580
581
582
583
584
585
586
587
588
589
590
591
592
593
594
595
596
597
598
599
600
601
602
603
604
605
606
607
608
609
610
611
612
613
614
615
616
617
618
619
620
621
622
623
624
625
626
627
628
629
630
631
632
633
634
635
636
637
638
639
640
641
642
643
644
645
646
647
648
649
650
651
652
653
654
655
656
657
658
659
660
661
662
663
664
665
666
667
668
669
670
671
672
673
674
675
676
677
678
679
680
681
682
683
684
685
686
687
688
689
690
691
692
693
694
695
696
697
698
699
700
701
702
703
704
705
706
707
708
709
710
711
712
713
714
715
716
717
718
719
720
721
722
723
724
725
726
727
728
729
730
731
732
733
734
735
736
737
738
739
740
741
742
743
744
745
746
747
748
749
750
751
752
753
754
755
756
757
758
759
760
761
762
763
764
765
766
767
768
769
770
771
772
773
774
775
776
777
778
779
780
781
782
783
784
785
786
787
788
789
790
791
792
793
794
795
796
797
798
799
800
801
802
803
804
805
806
807
808
809
810
811
812
813
814
815
816
817
818
819
820
821
822
823
824
825
826
827
828
829
830
831
832
833
834
835
836
837
838
839
840
841
842
843
844
845
846
847
848
849
850
851
852
853
854
855
856
857
858
859
860
861
862
863
864
865
866
867
868
869
870
871
872
873
874
875
876
877
878
879
880
881
882
883
884
885
886
887
888
889
890
891
892
893
894
895
896
897
898
899
900
901
902
903
904
905
906
907
908
909
910
911
912
913
914
915
916
917
918
919
920
921
922
923
924
925
926
927
928
929
930
931
932
933
934
935
936
937
938
939
940
941
942
943
944
945
946
947
948
949
950
951
952
953
954
955
956
957
958
959
960
961
962
963
964
965
966
967
968
969
970
971
972
973
974
975
976
977
978
979
980
981
982
983
984
985
986
987
988
989
990
991
992
993
994
995
996
997
998
999
1000

Anyway, there is no sufficient experimental evidence that confirm the oxidation of Co^{2+} to Co^{3+} during the chemical synthesis of $CoFe_2O_4$ NPs⁵¹. Hence, the precise distribution of 2+ and 3+ charges of Fe and Co cations of Co doped ferrites is still a matter of debate, which cannot be explained only by the charge balance of the unit cell, but further experiments are required.

1
2
3 In any case, the theoretical calculations are in good agreement with the experimental results
4 and confirm a partially inverted spinel structure, as expected for CoFe_2O_4 NPs.
5
6

7
8 Oxygen K-edge XAS spectra of all the MNPs dried films were also recorded both in TEY and
9 TFY mode and provided with further details in Figure S1 in the S.I.. The main features of the
10 spectra can be assigned to O 2p hybridized with the Fe and Co 3d (530 and 534 eV) and 4sp
11 states (536-544 eV). These components, which are typical of oxides such as CoFe_2O_4 ⁵²⁻⁵⁵, are
12 visible in all the samples, indicating that the main signal arises from the NPs cores, where the
13 contribution of the metal oxide is dominant with respect to the surface components responsible
14 for different charges and coatings.
15
16
17
18
19
20
21
22
23

24 The surface chemical composition of the NPs was also examined by photoemission. XPS
25 spectra of Fe 2p and Co 2p core levels of the three NP samples (Figure S2 (a) and (b),
26 respectively, in the S.I.) further confirm the oxidation state of the two metallic cations in
27 CoFe_2O_4 , and the superposition of the spectra clearly demonstrate that both the citrate coating
28 and surface charges do not affect the oxidation states.
29
30
31
32
33
34
35

36 More precisely, the position and separation of Fe $2p_{3/2}$ (710.4 eV) and $2p_{1/2}$ (724eV) peaks, and
37 the presence of the corresponding shake-up satellites at 718.9 eV and 733 eV, respectively,
38 indicate that the dominant state of Fe ions is +3⁵⁵⁻⁵⁷, however the broad band at 710.4 eV may
39 indicate also the presence of some Fe^{2+} ⁴². In the case of Co 2p, the peak at 780.6 eV with its
40 satellite at 786.6 eV, and the peak at 796.7 eV with its satellite at 803 eV are indicative of Co in
41 the +2 state⁵⁶⁻⁵⁸. The stoichiometric ratio between Fe and Co, quantified by using the intensity
42 of Fe 2p and Co 2p peaks and taking into account the cross sections of the two elements at the
43 current photon energy, was estimated to be close to 2:1 as expected for CoFe_2O_4 .
44
45
46
47
48
49
50
51
52
53
54
55
56
57
58
59
60

1
2
3 The high surface sensitivity of the O 1s XPS spectra obtained with the photon energy of 734
4 eV allowed us to investigate oxygen-containing species present on the surfaces of the NPs. The
5
6 O 1s spectra of the three samples shown in Figure 6 and Figure S3 (see S.I.) revealed different
7
8 chemical composition of the superficial layers adsorbed on the three types of NPs. All spectra are
9
10 broadened at higher binding energies, indicating the presence of several different oxygen species.
11
12 In order to identify the different groups containing oxygen, we decomposed the O 1s spectrum
13
14 into four components using Voigt shape peaks of similar width. The main O 1s peak centered at
15
16 529.9 eV, common for all samples, corresponds to O_2^- anions in the $CoFe_2O_4$ spinel crystal
17
18 lattice⁵⁸. Other two components, present for all the NP samples have been found at the binding
19
20 energy (BE) of 532.1 and 533 eV. The former can be associated with surface and near-surface
21
22 defect sites with low oxygen coordination, often formally described as O^- species^{59,60}. The latter
23
24 component can be assigned to water adsorbed during the sample preparation^{61,62} and to the
25
26 oxygen from the SiO_2 substrate carrying the NPs, as can be seen by comparing the O 1s spectrum
27
28 measured on bare substrate (Figure 6d). In the case of positively charged $CoFe_2O_4$ NPs, another
29
30 significant component was observed at the BE of 531.4 eV (Figure 6a). This component can be
31
32 assigned to the OH_3^+ ions adsorbed on the NP surface. Negatively charged NPs (Figure 6b)
33
34 revealed an extra component at the BE of 531.3 eV that can be assigned to the hydroxylate OH^-
35
36 groups responsible for the negative surface charge. The O 1s spectrum of the citrate coated NPs
37
38 (Figure 6c) showed spectral shape similar to the spectrum of negatively charged particles, which
39
40 were used as precursor for the coated NPs. However, the shape of the spectrum indicates a new
41
42 component at the BE of 531.1 eV. This peak can be attributed to the presence of COO^-
43
44 carboxylate groups^{61,63,64}. The carboxylate component implies that the citrate molecules were
45
46 bonded to the NPs in bidentate form⁶¹. Nonetheless, the monodentate form with C=O carbonyl
47
48
49
50
51
52
53
54
55
56
57
58
59
60

group cannot be excluded because the corresponding O 1s binding energy is expected at 532.3 eV^{26,63} and it could overlap with the O⁻ component. The capping citrate contains also -OH groups. The corresponding peak is expected around 532.9 eV^{26,63} which overlaps with the component from the SiO₂ support.

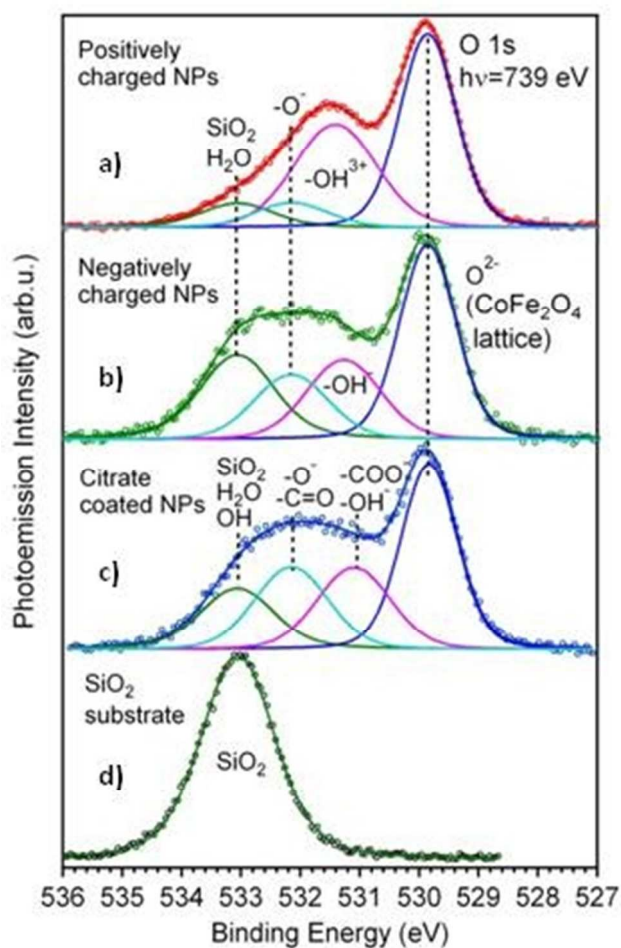
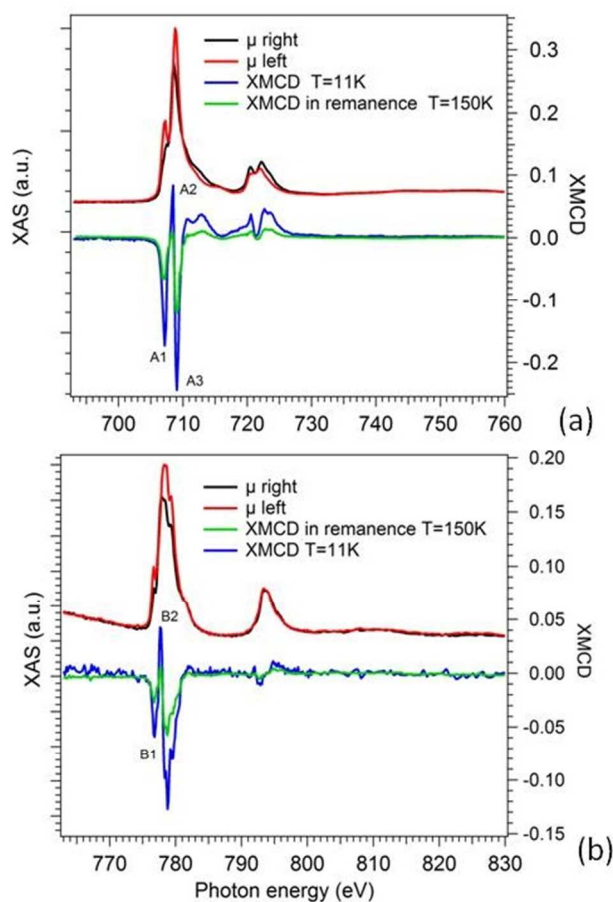


Figure 6. O 1s photoemission spectra obtained from negatively charged NPs (a), positively charged NPs (b), citrate coated NPs (c) and bare substrate carrying the NPs (d). The spectra were acquired using 734 eV photon energy. The experimental data (circles) were fitted with four spectral components (solid curves).

Magnetic characterization. The magnetic contributions of each cation (Co and Fe) and further information about the cationic distribution into CoFe₂O₄ NPs were obtained by XMCD

1
2
3 measurements under an applied magnetic field of 2 T at a temperature of 11 K and in the
4
5
6 remnant magnetization condition at 150 K.

7
8 In Figure 7 (a,b), Fe $L_{3,2}$ and Co $L_{3,2}$ edge XAS spectra of CoFe_2O_4 NPs are reported with the
9
10 photo-helicity of incident X-rays parallel ($\mu+$) and anti-parallel ($\mu-$) to the direction of
11
12 magnetization, and the corresponding XMCD are displayed as well. Fe and Co right-polarized
13
14 XAS spectra ($\mu+$) are shown with the absorption intensity of L_3 maximum normalized to 1 and
15
16 the left-polarized ($\mu-$) spectra scaled accordingly. XMCD spectra were then obtained by
17
18 subtracting the normalized XAS spectrum measured at opposite helicities. A strong magnetic
19
20 dichroism is observed for both metals, and the general line shapes are consistent with those
21
22 reported in the literature^{44,49,50}.



1
2
3 **Figure 7.** XAS (right and left photon helicity) and the corresponding magnetic difference
4 XMCD spectra of uncoated CoFe_2O_4 NPs at the Fe $L_{3,2}$ (a) and Co $L_{3,2}$ edge (b) measured both at
5
6 11 K under an applied magnetic field of 2 T and at 150 K at remanence.
7
8

9
10
11 The XMCD spectra of Fe $L_{3,2}$ region (Figure 7a) show two negative peaks at 707.2 (A1) and
12 709 eV (A3) corresponding to Fe^{2+} and Fe^{3+} ions at the O_h sites, whereas the positive peak at
13 708.6 eV (A2) corresponds to the Fe^{3+} cations occupying the T_d sites. The opposite directions of
14 the features A1 and A3 with respect to A2 arise from the antiferromagnetic interaction of the Fe
15 ions at the O_h and T_d sites, while the same directions of the peaks A1 and A3 reflects the
16 ferromagnetic interaction between Fe^{2+} and Fe^{3+} in the O_h site.
17
18

19
20
21 In the case of Co $L_{3,2}$ edge, the XMCD spectra in Figure 7 (b) show a strong negative peak at
22 779.3 eV (B1), and a positive one at 778.1 eV (B2). The feature B1 at 779.3 eV corresponds to
23 Co^{2+} cations at the O_h sites, while the positive peak B2 at 778.5 eV corresponds to Co^{2+} located
24 at the T_d sites. The opposite directions of features B1 and B2 reflect the antiferromagnetic
25 interaction of Co^{2+} cations at the O_h and T_d sites. A comparison between Co and Fe XMCD
26 spectra clearly indicates that Co^{2+} O_h cations are ferromagnetically coupled to Fe^{2+} and Fe^{3+} O_h
27 cations.
28
29

30
31
32 The spectra under remnant magnetization conditions clearly show that the CoFe_2O_4 NPs
33 preserved a fairly large magnetization after the field removal even at higher temperature (150 K).
34

35
36
37 The experimental XMCD spectra of Fe $L_{3,2}$ and Co $L_{3,2}$ were compared to those calculated by
38 LFM model, using the same Slater integrals reduced to 80% adopted for XAS simulation (see
39 above), and a Lorentzian half-width of 0.2(0.3) eV and a Gaussian half-width of 0.15 eV.
40
41

42
43
44 The calculations of XMCD data confirm the partially inverted spinel structure of CoFe_2O_4 NPs
45 extrapolated also from XAS spectra.
46
47
48
49
50
51
52
53
54
55
56
57
58
59
60

Figure 8 shows the Fe $L_{3,2}$ (a) and Co $L_{3,2}$ (b) XMCD spectra together with the simulated ones obtained from the linear combination of the LFM calculated spectra of the single cations distributed among the Oh and Td sites.

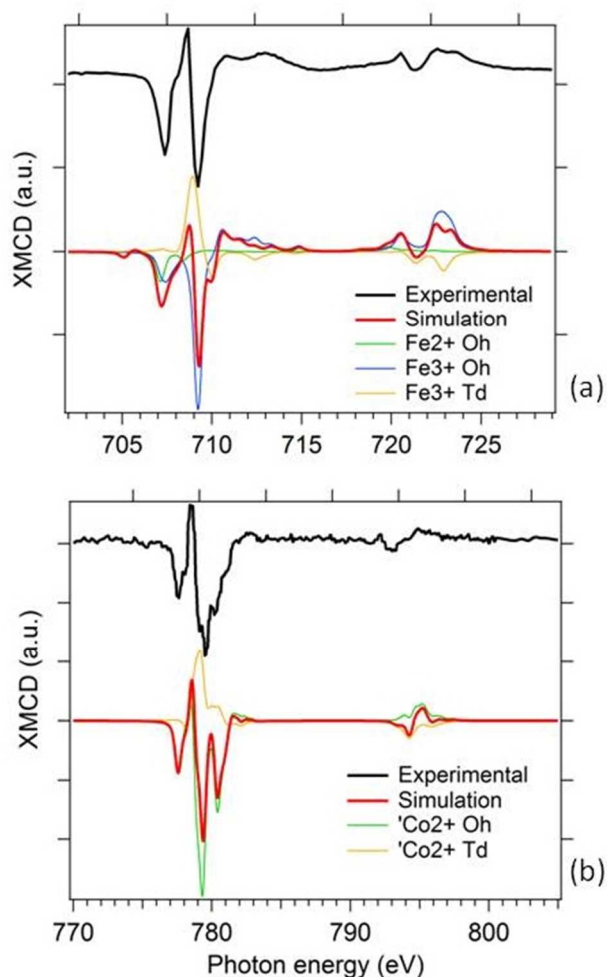


Figure 8. Comparison between the calculated LFM spectra (red curves) and the experimental XMCD spectra (black curves) of Fe $L_{3,2}$ edge (a) and Co $L_{3,2}$ edge (b) of CoFe_2O_4 NPs. The calculated spectral components corresponding to Fe^{3+} Oh, Fe^{3+} Td and Fe^{2+} Oh cations, and Co^{2+} Oh and Co^{2+} Td cations, respectively, are displayed as well.

As expected, the combination of individual cationic spectra used for the calculation of Fe $L_{3,2}$ XMCD spectrum fit pretty well with those used for the simulation of Fe $L_{3,2}$ XAS spectrum,

confirming 71% of Fe³⁺ ions at the Oh sites, 19% of Fe³⁺ cations at the Td sites, and 10% of Fe²⁺ species at the Oh sites. Similarly, the calculation of the theoretical Co L_{3,2} XMCD spectrum simulates quite well the overall Co L_{3,2} XMCD experimental spectrum, if the Co²⁺ Oh and Td components are taken in the same proportions as those determined from the XAS analysis (75 and 25%, respectively). Quantative information from XMCD data can be obtained by using the "sum rules" analysis that relate the integration of the XAS and XMCD⁴⁸ spectra with the orbital (m_L) and spin (m_S) magnetic moments by the following equations⁶⁵⁻⁶⁷:

$$m_L = -4q(10-n_{3d})/3r \quad (1)$$

$$m_S = -(6p-4q)(10-n_{3d})/r \quad (2)$$

where m_L and m_S are given in units of Bohr magnetons per cation (μ_B /cation), and n_{3d} is the 3d electron occupation number per specific cation. The n_{3d} values used for the calculation are 5.6 for Fe, and 7.21 for Co ions, which are expected for Co_(1-x)Fe_(2+x)O₄ magnetic structures⁴⁸.

The values of p and q were extracted from the integration of the calculated XMCD spectra (see Figure S4 in S.I.), and the r value by integrating the simulated isotropic XAS spectra of Fe and Co (see Figure S5 in S.I.). Generally, the "sum rules" are applied to one specific transition, i.e. the transition from a 2p core state to 3d valence states in transition metal (TM) systems.

The m_L and m_S of Fe and Co obtained from the sum rules at the temperature of 11 K upon an applied magnetic field of 2 T in the direction parallel to the beam, and at the temperature of 150 K at remanence are reported in Table 3.

Table 3. Orbital (m_L) and spin magnetic (m_S) moments of Fe and Co atoms calculated from the overall XMCD spectra with sum rules.

T=11 K, H=2T	m_L (μ_B /cation)	m_S (μ_B /cation)	m_L/m_S	m_L+m_S (μ_B /cation)

Fe	0.075	1.21	0.062	1.28
Co	0.21	0.32	0.65	0.53
Tot CoFe₂O₄	0.36	2.74	0.19	3.10
T=150 K, remanence				
Fe	0.044	0.67	0.065	0.714
Co	0.101	0.15	0.67	0.251
Tot CoFe₂O₄	0.145 μ_B	1.49 μ_B	0.19 μ_B	1.64 μ_B

The magnetic moments of each single components of Fe and Co distributed among *Td* and *Oh* sites were also calculated with the XMCD sum rules applied to the single simulated spectra at saturation (see Table 4). The n_{3d} values were considered 5 and 6 for Fe³⁺ and Fe²⁺ cations, respectively, and 7 for Co²⁺ cations. Combining the magnetic moments for the corresponding occupational contribution, we have obtained the total magnetic moments, which are comparable to those calculated from the overall XMCD Fe and Co spectra at 11 K and 2 T.

Table 4. Orbital (m_L) and spin magnetic (m_S) moments of each Fe component (Fe³⁺ *Oh*, Fe³⁺ *Td* and Fe²⁺ *Oh*) and Co component (Co²⁺ *Td* and Co²⁺ *Oh*) calculated with XMCD sum rules at saturation.

XMCD at saturation	m_L (μ_B/cation)	m_S (μ_B/cation)	m_L/m_S	m_L+m_S (μ_B/cation)
Fe ³⁺ <i>Oh</i>	0.02	1.89	0.01	1.91
Fe ³⁺ <i>Td</i>	-0.013	-1.81	0.007	-1.82
Fe ²⁺ <i>Oh</i>	0.46	1.62	0.28	2.017
Fe	0.058	1.16	0.05	1.22

$\text{Co}^{2+} \text{ Oh}$	0.35	0.76	0.46	1.11
$\text{Co}^{2+} \text{ Td}$	-0.16	-1.12	0.14	-1.28
Co	0.22	0.29	0.75	0.51
Tot CoFe_2O_4	0.34 μ_B	2.61 μ_B	0.13 μ_B	2.95 μ_B

The calculated orbital and spin components indicate a m_L close to zero for Fe cations (quenching of the orbital moment) in line with those reported in literature for $\text{Co}_{(1-x)}\text{Fe}_{(2+x)}\text{O}_4$ ⁴⁸ and Fe_3O_4 NPs^{48,68}; while the values of m_S are higher than the m_S reported by Moyer et al. for bulk $\text{Co}_{(1-x)}\text{Fe}_{(2+x)}\text{O}_4$ ⁴⁸, but comparable to the values calculated by Y. P. Cai et al for Fe_3O_4 NPs⁶⁸.

On the other hand, for Co ions the orbital and spin components are comparable (but slightly lower) to those reported in literature for "bulk" CoFe_2O_4 film⁴⁸.

The enhanced total magnetic moment of Fe in CoFe_2O_4 NPs can be associated to a dominant concentration of Fe cations in the unit cell, as also observed by Moyer et al.⁴⁸, who showed an increase of Fe magnetic moments with increasing x in $\text{Co}_{(1-x)}\text{Fe}_{(2+x)}\text{O}_4$ structure. In fact, this hypothesis could confirm our theoretical results from XAS spectra, indicating that the ratio between Fe and Co is higher than 2 (2.12 from ICP-AES measurements). Most likely, the excess of Fe replaced the lack of Co^{2+} ions as Fe^{2+} ions at the Oh sites^{42,48}.

Another possible reason that could explain the differences between the magnetic moments obtained by Moyer et al⁴⁸ on CoFe_2O_4 thin film and our results on CoFe_2O_4 NPs can be associated to nano-structural effects in nanoparticles, resulting from their reduced size. The curvature and the large surface area imply that more cations are located at the surface, resulting in a more disordered distribution of the electron spins because of their reduced spin-spin exchange^{17,18}. In addition to the nanometric size, also the preparation method of CoFe_2O_4 NPs

1
2
3 can lead to an increased fractional volume of an oxidized shell at the surface of the NPs, which
4
5 could contribute to change the orbital moments of Fe⁶⁸.
6
7

8 As expected, the orbital and spin components of both Fe and Co atoms are lower at 150 K in
9
10 remnant magnetization than at 11 K upon an applied magnetic field of 2 T, and their ratio m_I/m_S
11
12 remain unchanged.
13
14

15 Magnetometry hysteresis loops measured at 2.5 K on the three CoFe₂O₄ NP samples are
16
17 reported in Figure 9. The coating does not influence appreciably the magnetic properties of the
18
19 NPs, as can be seen from the values of coercivity (~0.85 T) and relative remnant magnetization
20
21 (~0.7 T), as well as from the approach to saturation of the curves. This is not surprising since the
22
23 high magneto-crystalline anisotropy of cobalt ferrite makes possible changes of surface
24
25 contribution negligible. The saturation magnetization values are 64 Am²/kg (negative), 68
26
27 Am²/kg (positive) and 73 Am²/kg (citrate). The minor differences in the saturation magnetization
28
29 values between the three samples can be ascribed to the uncertainty in the determination of the
30
31 effective concentration of NPs in the dispersion, as opposed to ligands and residual solvent.
32
33
34
35

36 The total magnetic moments measured with SQUID magnetometry (2.69 μ_B for negative, 2.86
37
38 μ_B for positive, and 3.08 μ_B for citrate) are in good agreement with those calculated for uncoated
39
40 CoFe₂O₄ NPs from XMCD spectra at 11 K and 2 T (3.09 μ_B, Table 3) and from the linear
41
42 combination of the calculated single magnetic moments at saturation (2.95 μ_B, Table 4).
43
44
45
46
47
48
49
50
51
52
53
54
55
56
57
58
59
60

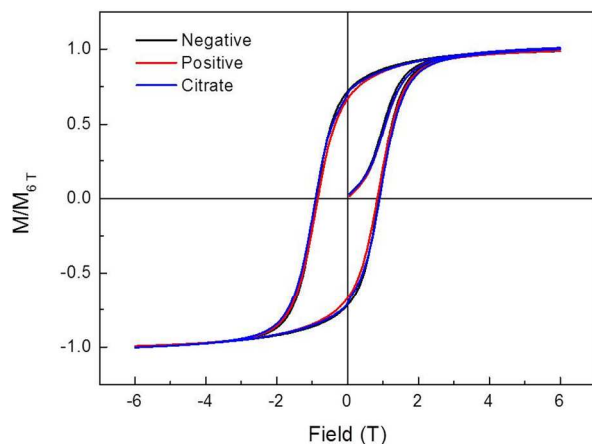


Figure 9. Normalized magnetization curves of negative, positive and citrate-coated CoFe_2O_4 NPs measured at 2.5 K.

Magnetic hysteresis loops on the same samples were previously acquired at 310 K in order to understand the magnetic behavior of CoFe_2O_4 NPs dispersed in aqueous solution at room temperature, giving important information on their biological and clinic applicability⁶. A weaker applied field was found to be enough to align all citrate coated MNPs, pointing out the important role of the citrate capping in preventing the formation of aggregates in aqueous solution, making citrate coated MNPs more suitable for clinical applications. On the other hand, hysteresis loops measured at 310 K on the three samples in the solid state showed that a small coercivity is present at room temperature (~ 250 Oe, see Figure S6 in S. I.); this suggests that high thermal losses are to be expected at the alternating field frequency typical of the magnetic fluid hyperthermia (see below).

One of the most promising clinical applications of magnetic NPs is magnetic fluid hyperthermia (MFH), i.e. the selective destruction of tumor cells by exploiting the heat released from the inorganic core under the application of an alternating magnetic field (AMF). In order to evaluate the heating efficiency of the three CoFe_2O_4 NPs samples, the temperature kinetics

1
2
3 during five minutes of exposition to an AMF (17 kA/m, 183 kHz) were measured, and their
4
5 specific absorption rate (SAR) results are reported in Figure 10.
6
7

8 The SAR values, evaluated from the initial slopes of the curves, were found comparable for
9
10 negative and positive CoFe₂O₄ NPs, being 105 ± 3 and 98 ± 4 W/g of total metals (Fe + Co),
11
12 respectively.
13
14

15 However, a reduction of SAR to 65 ± 7 W/g of total metals (Fe + Co) was observed for the
16
17 citrate-coated sample. In order to shed light on the relaxation mechanism involved in the heat
18
19 generation, the Néel and Brownian relaxation times were estimated according to the work of
20
21 Rosensweig⁶⁹. The Néel relaxation time (τ_N) was calculated using the formula
22
23

$$24 \tau_N = \frac{\sqrt{\pi}}{2} \tau_0 \frac{\exp(KV/k_B T)}{\sqrt{KV/k_B T}}$$

25
26
27
28
29

30 where V is nanoparticle volume from TEM characterization, K the anisotropy constant of
31
32 cobalt ferrite (1.2 10⁵ J/m³)⁷⁰ and τ_0 the exponential factor (10⁻⁹ s).
33
34

35 The calculation of the Brownian relaxation time (τ_B) was performed by using the formula
36
37

$$38 \tau_B = \frac{3\eta V_H}{k_B T}$$

39
40
41

42 where V_H is the hydrodynamic volume (calculated considering the hydrodynamic radii reported
43
44 in our previous work⁶) and η the viscosity coefficient of water. The obtained data shows that the
45
46 relaxation time of Néel mechanism is considerably smaller than the Brown one for all the three
47
48 samples. Thus the magnetization reversal above the energy barrier can be considered the
49
50 dominant mechanism. In this framework, the small change in hydrodynamic radius induced by
51
52 the ligand modification cannot be responsible for the different hyperthermic efficiency of the
53
54 samples. This result is corroborated by previously published AC susceptibility measurements⁶ on
55
56
57
58
59
60

aqueous dispersions of the citrate coated NPs which clearly showed that the NPs were not mechanically affected by the oscillating magnetic field. Thus, by also taking into account that the magnetic investigation shows very similar magnetic parameters for all the samples, such discrepancy can be ascribed to a different efficiency in stabilizing NPs by the different surface coatings.

The steric effect of citrate molecules combined with the charge repulsion related to the negatively charged carboxylate groups is indeed expected to improve the stabilization of the citrate-coated CoFe_2O_4 NPs, by increasing the average separation between particles, thus reducing the dipolar interactions. The effect of magnetic interactions on hyperthermic efficiency is still under debate⁷¹. Recently, a theoretical study by Burrows et al.⁷² reported an increase of the energy losses with interactions for superparamagnetic NPs, due to the enhancement of the energy barrier due to dipole-dipole interactions. In this framework then, it is possible to attribute the higher SAR values observed for negatively and positively charged CoFe_2O_4 NPs to the presence of a higher degree of dipolar interactions, due to a less efficient particle stabilization with respect to the citrate-coated sample.

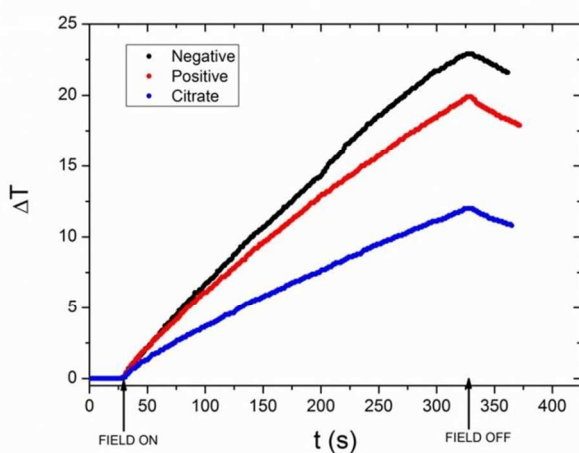


Figure 10. Temperature kinetic curves of CoFe_2O_4 NP samples during the exposition to an alternating magnetic field (17 kA/m, 183 kHz, 5 min), starting from a temperature of 25°C.

4. Conclusions

A simple approach based on co-precipitation method was used for the preparation of CoFe_2O_4 colloidal spherical NPs with mean diameter of 12 nm. Different stabilization methodologies were used to obtain well-dispersed MNPs in aqueous solution, exploiting both the electrostatic repulsion of uncoated NPs with different surface charge (positive and negative), and a capping agent (citric acid).

The paper reports a detailed spectroscopic characterization of the three investigated MNP samples (positively and negatively charged uncoated MNPs, and citrate coated MNPs) deposited as thin films on Si wafers. In particular, the electronic properties and the oxidation states of the metal ions of CoFe_2O_4 NPs were probed by XAS and XPS experiments, confirming that Fe is present dominantly in the +3 state, while Co is in the +2 state for all the samples. The functionalization of CoFe_2O_4 NPs by interaction with citric acid was proved by ATR-FTIR and XPS measurements, revealing chemisorption of citrate ions and coordination via one or two of the carboxylate functionalities on the NP surface.

XMCD and XAS absorption spectra at the $L_{3,2}$ edge of Fe and Co have revealed the presence of a small amount of Fe^{2+} ions located at the O_h sites, while the dominant Fe^{3+} and Co^{2+} cations occupy both the O_h and T_d sites. Finally, hysteresis loops at low temperature were carried out, showing that both uncoated and citrate-coated CoFe_2O_4 NPs have a similar magnetic behavior, confirming that the citrate layer does not affect the total anisotropy of the particles. However, the lower SAR value observed for citrate-coated CoFe_2O_4 NPs with respect to the negative and positive ones suggests that the hyperthermic properties are influenced by the efficiency of the surface coating in stabilizing the NPs suspension.

1
2
3 In the light of our results, we can conclude that the surface charge and the coating shell of
4 citrate do not alter the electronic properties and the distribution of Fe and Co cations in the oxide
5 cores, and also the magnetic properties remain unchanged. On the other hand, the influence of
6 coating molecules on the hyperthermic efficiency of the nanoparticles deserves further
7 investigation that goes beyond the scope of this paper. It should be stressed, however, that the
8 thorough investigation carried out here restricts any effect of the coating to particle dispersibility,
9 as opposed to alterations of the particle core. This represents an important result for biomedical
10 applications of CoFe_2O_4 NPs.
11
12

13
14
15 In view of these considerations, our results are the groundwork for future investigations in a
16 liquid environment, aimed at studying how the dispersibility of MNPs in a solvent might perturb
17 the electronic and magnetic properties of coated and uncoated MNPs. The development of
18 special cells consisting of window membranes resistant to UHV conditions and transparent to x-
19 ray photons⁷³⁻⁷⁶ could open the possibility to study MNPs directly in physiological conditions,
20 that is the typical environment required for biomedical applications.
21
22
23
24
25
26
27
28
29
30
31
32
33
34
35
36
37
38

39 ABBREVIATIONS

40 NPs nanoparticles; MNPs magnetic nanoparticles; XAS x-ray absorption spectroscopy; XMCD
41 x-ray magnetic circular dichroism; XPS x-ray photoemission spectroscopy; ATR-FTIR
42 attenuated total reflection infrared spectroscopy; VSM vibrating sample magnetometer; AMF
43 Alternating Magnetic Field; UHV ultra-high vacuum; TEY total electron yield; TFY total
44 fluorescence yield; SAXS Small Angle X-ray Scattering; TEM Transmission Electron
45 Microscopy; AC alternating current; MFH magnetic fluid hyperthermia, MRI magnetic
46 resonance imaging; TMAH tetramethyl-ammonium hydroxide; BE binding energy.
47
48
49
50
51
52
53
54
55
56
57
58
59
60

1
2
3 ACKNOWLEDGMENT
4

5 The authors thank Federico Salvador and Paolo Bertoch for technical support. This work was
6 financially supported by the START-UP project IOM-CNR , MIUR (FIRB project Riname
7 RBAP114AMK and FIRB Futuro in Ricerca 2012: RBFR128BEC) and INSTM-Regione
8 Lombardia (project "MAGNANO").
9

10
11 ASSOCIATED CONTENT
1213
14
15 **Supporting Information.**
16

17
18
19
20
21
22
23 Details about the concentration, XAS and XPS spectra of CoFe_2O_4 NPs, and the analysis of
24 XMCD and XAS spectra for the application of the sum rules are reported in the Supplementary
25 Information (S.I.). This material is available free of charge via the Internet at <http://pubs.acs.org>.
26
27
28
29

30
31 AUTHOR INFORMATION
3233 **Corresponding Author**
34

35
36 Dr. Silvia Nappini*

37
38
39 * e-mail: nappini@iom.cnr.it; tel: +39 040 375 8698; fax: +39 040 226 767
40
41

42
43 **Author Contributions**
44

45 The manuscript was written through contributions of all authors. All authors have given approval
46 to the final version of the manuscript.
47
48

49
50
51 **Notes**
52

53 The authors declare no competing financial interest
54
55

56
57 REFERENCES
58
59
60

- 1
2
3 (1) Reiss, G.; Hütten, A. Magnetic Nanoparticles: Applications beyond Data Storage. *Nat.*
4
5 *Mater.* **2005**, *4*, 725–726.
6
7
8
9 (2) Hyeon, T. Chemical Synthesis of Magnetic Nanoparticles. *Chem. Commun.* **2003**, 927–
10
11 934.
12
13
14 (3) Lu, A.-H.; Schmidt, W.; Matoussevitch, N.; Bönemann, H.; Spliethoff, B.; Tesche, B.;
15
16 Bill, E.; Kiefer, W.; Schüth, F. Nanoengineering of a Magnetically Separable Hydrogenation
17
18 Catalyst. *Angew. Chem.* **2004**, *116*, 4403–4406.
19
20
21
22 (4) Tsang, S. C.; Caps, V.; Paraskevas, I.; Chadwick, D.; Thompsett, D. Magnetically
23
24 Separable, Carbon-Supported Nanocatalysts for the Manufacture of Fine Chemicals. *Angew.*
25
26 *Chem. Int. Ed.* **2004**, *43*, 5645–5649.
27
28
29
30 (5) Li, S.; Ding, W.; Meitzner, G. D.; Iglesia, E. Spectroscopic and Transient Kinetic Studies
31
32 of Site Requirements in Iron-Catalyzed Fischer–Tropsch Synthesis. *J. Phys. Chem. B* **2002**, *106*,
33
34 85–91.
35
36
37
38 (6) Nappini, S.; Bonini, M.; Bombelli, F. B.; Pineider, F.; Sangregorio, C.; Baglioni, P.;
39
40 Nordèn, B. Controlled Drug Release under a Low Frequency Magnetic Field: Effect of the
41
42 Citrate Coating on Magnetoliposomes Stability. *Soft Matter* **2011**, *7*, 1025–1037.
43
44
45
46 (7) Nappini, S.; Bombelli, F. B.; Bonini, M.; Nordèn, B.; Baglioni, P. Magnetoliposomes for
47
48 Controlled Drug Release in the Presence of Low-Frequency Magnetic Field. *Soft Matter* **2009**, *6*,
49
50 154–162.
51
52
53
54
55
56
57
58
59
60

1
2
3 (8) Douziech-Eyrolles, L.; Marchais, H.; Herve, K.; Munnier, E.; Souce, M.; Linassier, C.;
4
5 Dubois, P.; Chourpa, I. Nanovectors for Anticancer Agents Based on Superparamagnetic Iron
6
7 Oxide Nanoparticles. *Int. J. Nanomedicine* **2007**, *2*, 541–550.

8
9
10
11 (9) Tartaj, P.; Morales, M. del P.; Veintemillas-Verdaguer, S.; González-Carreño, T.; Serna,
12
13 C. J. The Preparation of Magnetic Nanoparticles for Applications in Biomedicine. *J. Phys. Appl.*
14
15 *Phys.* **2003**, *36*, R182-R197.

16
17
18
19 (10) Huang, J. Improving the Magnetic Resonance Imaging Contrast and Detection Methods
20
21 with Engineered Magnetic Nanoparticles. *Theranostics* **2012**, *2*, 86–102.

22
23
24 (11) Chen, S.; Chiang, C.; Hsieh, S. Simulating Physiological Conditions to Evaluate
25
26 Nanoparticles for Magnetic Fluid Hyperthermia (MFH) Therapy Applications. *J. Magn. Magn.*
27
28 *Mater.* **2010**, *322*, 247–252.

29
30
31
32 (12) Ito, A.; Takizawa, Y.; Honda, H.; Hata, K.; Kagami, H.; Ueda, M.; Kobayashi, T. Tissue
33
34 Engineering Using Magnetite Nanoparticles and Magnetic Force: Heterotypic Layers of
35
36 Cocultured Hepatocytes and Endothelial Cells. *Tissue Eng.* **2004**, *10*, 833–840.

37
38
39 (13) Franco, A.; Machado, F. L. A.; Zapf, V. S. Magnetic Properties of Nanoparticles of
40
41 Cobalt Ferrite at High Magnetic Field. *J. Appl. Phys.* **2011**, *110*, 053913–053913 – 6.

42
43
44 (14) Carta, D.; Casula, M. F.; Falqui, A.; Loche, D.; Mountjoy, G.; Sangregorio, C.; Corrias,
45
46 A. A Structural and Magnetic Investigation of the Inversion Degree in Ferrite Nanocrystals
47
48 MFe_2O_4 (M = Mn, Co, Ni). *J. Phys. Chem. C* **2009**, *113*, 8606–8615.
49
50
51
52
53
54
55
56
57
58
59
60

1
2
3 (15) Li, S.; Liu, L.; John, V. T.; O'Connor, C. J.; Harris, V. G. Cobalt-Ferrite Nanoparticles:
4 Correlations between Synthesis Procedures, Structural Characteristics and Magnetic Properties.
5
6 *IEEE Trans. Magn.* **2001**, *37*, 2350–2352.
7
8

9
10
11 (16) Schultz-Sikma, E. A.; Joshi, H. M.; Ma, Q.; MacRenaris, K. W.; Eckermann, A. L.;
12 Dravid, V. P.; Meade, T. J. Probing the Chemical Stability of Mixed Ferrites: Implications for
13
14 Magnetic Resonance Contrast Agent Design. *Chem. Mater.* **2011**, *23*, 2657–2664.
15
16
17

18
19 (17) Nordhei, C.; Ramstad, A. L.; Nicholson, D. G. Nanophase Cobalt, Nickel and Zinc
20
21 Ferrites: Synchrotron XAS Study on the Crystallite Size Dependence of Metal Distribution.
22
23 *Phys. Chem. Chem. Phys.* **2008**, *10*, 1053–1066.
24
25
26

27 (18) Jun, Y.-W.; Seo, J.-W.; Cheon, J. Nanoscaling Laws of Magnetic Nanoparticles and
28
29 Their Applicabilities in Biomedical Sciences. *Acc. Chem. Res.* **2008**, *41*, 179–189.
30
31

32 (19) Sahoo, Y.; Pizem, H.; Fried, T.; Golodnitsky, D.; Burstein, L.; Sukenik, C. N.;
33
34 Markovich, G. Alkyl Phosphonate/Phosphate Coating on Magnetite Nanoparticles: A
35
36 Comparison with Fatty Acids. *Langmuir* **2001**, *17*, 7907–7911.
37
38
39

40 (20) Wooding, A.; Kilner, M.; Lambrick, D. B. Studies of the Double Surfactant Layer
41
42 Stabilization of Water-Based Magnetic Fluids. *J. Colloid Interface Sci.* **1991**, *144*, 236–242.
43
44
45

46 (21) Zhang, Y.; Kohler, N.; Zhang, M. Surface Modification of Superparamagnetic Magnetite
47
48 Nanoparticles and Their Intracellular Uptake. *Biomaterials* **2002**, *23*, 1553–1561.
49
50

51 (22) Studart, A. R.; Amstad, E.; Gauckler, L. J. Colloidal Stabilization of Nanoparticles in
52
53 Concentrated Suspensions. *Langmuir* **2007**, *23*, 1081–1090.
54
55
56
57
58
59
60

1
2
3 (23) Laurent, S.; Forge, D.; Port, M.; Roch, A.; Robic, C.; Vander Elst, L.; Muller, R. N.
4
5
6
7
8
9
10
11
12
13
14
15
16
17
18
19
20
21
22
23
24
25
26
27
28
29
30
31
32
33
34
35
36
37
38
39
40
41
42
43
44
45
46
47
48
49
50
51
52
53
54
55
56
57
58
59
60

Magnetic Iron Oxide Nanoparticles: Synthesis, Stabilization, Vectorization, Physicochemical Characterizations, and Biological Applications. *Chem. Rev.* **2008**, *108*, 2064–2110.

(24) Massart, R. Preparation of Aqueous Magnetic Liquids in Alkaline and Acidic Media. *IEEE Trans. Magn.* **1981**, *17*, 1247–1248.

(25) Bonini, M.; Wiedenmann, A.; Baglioni, P. Small Angle Polarized Neutrons (SANS POL) Investigation of Surfactant Free Magnetic Fluid of Uncoated and Silica-Coated Cobalt–Ferrite Nanoparticles. *J. Phys. Chem. B* **2004**, *108*, 14901–14906.

(26) Matthew, J. Surface Analysis by Auger and X-Ray Photoelectron Spectroscopy. D. Briggs and J. T. Grant (eds). IMPublications, Chichester, UK and SurfaceSpectra, Manchester, UK, 2003. 900 Pp., ISBN 1-901019-04-7, 900 Pp. *Surf. Interface Anal.* **2004**, *36*, 1647–1647.

(27) Stavitski, E.; de Groot, F. M. F. The CTM4XAS Program for EELS and XAS Spectral Shape Analysis of Transition Metal L Edges. *Micron* **2010**, *41*, 687–694.

(28) Singh, M. A.; Ghosh, S. S.; Shannon Jnr, R. F. A Direct Method of Beam-Height Correction in Small-Angle X-Ray Scattering. *J. Appl. Crystallogr.* **1993**, *26*, 787–794.

(29) Hergt, R.; Dutz, S. Magnetic Particle Hyperthermia—biophysical Limitations of a Visionary Tumour Therapy. *J. Magn. Magn. Mater.* **2007**, *311*, 187–192.

(30) Goertz, V.; Dingenouts, N.; Nirschl, H. Comparison of Nanometric Particle Size Distributions as Determined by SAXS, TEM and Analytical Ultracentrifuge. *Part. Part. Syst. Charact.* **2009**, *26*, 17–24.

1
2
3 (31) Bartlett, P.; Ottewill, R. H. A Neutron Scattering Study of the Structure of a Bimodal
4 Colloidal Crystal. *J. Chem. Phys.* **1992**, *96*, 3306–3318.
5
6

7
8
9 (32) Schulz, G. V. *Z. Phys. Chem.*, **1935**, *43*, 25.
10

11
12 (33) Hayter, J. B.; Penfold, J. An Analytic Structure Factor for Macroion Solutions. *Mol.*
13 *Phys.* **1981**, *42*, 109–118.
14
15

16
17 (34) Kohler, N.; Sun, C.; Wang, J.; Zhang, M. Methotrexate-Modified Superparamagnetic
18 Nanoparticles and Their Intracellular Uptake into Human Cancer Cells. *Langmuir* **2005**, *21*,
19 8858–8864.
20
21
22

23
24 (35) Mudunkotuwa, I. A.; Grassian, V. H. Citric Acid Adsorption on TiO₂ Nanoparticles in
25 Aqueous Suspensions at Acidic and Circumneutral pH: Surface Coverage, Surface Speciation,
26 and Its Impact on Nanoparticle-Nanoparticle Interactions. *J. Am. Chem. Soc.* **2010**, *132*, 14986–
27 14994.
28
29
30
31
32

33
34 (36) Cheraghipour, E. Citrate Capped Superparamagnetic Iron Oxide Nanoparticles Used for
35 Hyperthermia Therapy. *J. Biomed. Sci. Eng.* **2012**, *05*, 715–719.
36
37
38

39
40 (37) Sahoo, Y.; Goodarzi, A.; Swihart, M. T.; Ohulchansky, T. Y.; Kaur, N.; Furlani, E. P.;
41 Prasad, P. N. Aqueous Ferrofluid of Magnetite Nanoparticles: Fluorescence Labeling and
42 Magnetophoretic Control. *J. Phys. Chem. B* **2005**, *109*, 3879–3885.
43
44
45
46
47

48
49 (38) Răcuciu, M.; Creangă, D. E.; Airinei, A. Citric-Acid-Coated Magnetite Nanoparticles for
50 Biological Applications. *Eur. Phys. J. E* **2006**, *21*, 117–121.
51
52
53
54
55
56
57
58
59
60

1
2
3 (39) Nigam, S.; Barick, K. C.; Bahadur, D. Development of Citrate-Stabilized Fe₃O₄
4 Nanoparticles: Conjugation and Release of Doxorubicin for Therapeutic Applications. *J. Magn.*
5
6 *Magn. Mater.* **2011**, *323*, 237–243.
7
8

9
10
11 (40) Max, J.-J.; Chapados, C. Infrared Spectroscopy of Aqueous Carboxylic Acids:
12 Comparison between Different Acids and Their Salts. *J. Phys. Chem. A* **2004**, *108*, 3324–3337.
13
14

15
16
17 (41) Braun, A.; Bayraktar, D.; Erat, S.; Harvey, A. S.; Beckel, D.; Purton, J. A.; Holtappels,
18 P.; Gauckler, L. J.; Graule, T. Pre-Edges in Oxygen (1s) X-Ray Absorption Spectra: A Spectral
19 Indicator for Electron Hole Depletion and Transport Blocking in Iron Perovskites. *Appl. Phys.*
20 *Lett.* **2009**, *94*, 202102–202102 – 3.
21
22
23

24
25
26
27 (42) Moyer, J. A.; Vaz, C. A. F.; Negusse, E.; Arena, D. A.; Henrich, V. E. Controlling the
28 Electronic Structure of Co_{1-x}Fe_{2+x}O₄ Thin Films through Iron Doping. *Phys. Rev. B* **2011**, *83*,
29 035121–035121 – 10.
30
31
32

33
34
35 (43) Moyer, J. A.; Kumah, D. P.; Vaz, C. a. F.; Arena, D. A.; Henrich, V. E. Epitaxial Strain-
36 Induced Changes in the Cation Distribution and Resistivity of Fe-Doped CoFe₂O₄. *Appl. Phys.*
37 *Lett.* **2012**, *101*, 021907–021907 – 4.
38
39
40

41
42
43 (44) Wang, B. Y.; Wang, H. T.; Singh, S. B.; Shao, Y. C.; Wang, Y. F.; Chuang, C. H.; Yeh,
44 P. H.; Chiou, J. W.; Pao, C. W.; Tsai, H. M.; *et al.* Effect of Geometry on the Magnetic
45 Properties of CoFe₂O₄–PbTiO₃ Multiferroic Composites. *RSC Adv.* **2013**, *3*, 7884–7893.
46
47
48

49
50
51 (45) Schmitz-Antoniak, C.; Schmitz, D.; Borisov, P.; de Groot, F. M. F.; Stienen, S.; Warland,
52 A.; Krumme, B.; Feyerherm, R.; Dudzik, E.; Klemann, W.; *et al.* Electric in-Plane Polarization
53
54
55

1
2
3 in Multiferroic $\text{CoFe}_2\text{O}_4/\text{BaTiO}_3$ Nanocomposite Tuned by Magnetic Fields. *Nat. Commun.*
4
5 **2013**, *4*, 2051.
6

7
8
9 (46) Kuiper, P.; Searle, B. G.; Rudolf, P.; Tjeng, L. H.; Chen, C. T. X-Ray Magnetic
10
11 Dichroism of Antiferromagnet Fe_2O_3 : The Orientation of Magnetic Moments Observed by Fe 2p
12
13 X-Ray Absorption Spectroscopy. *Phys. Rev. Lett.* **1993**, *70*, 1549–1552.
14

15
16
17 (47) Kuiper, P.; Searle, B. G.; Duda, L.-C.; Wolf, R. M.; van der Zaag, P. J. Fe L_{2,3} Linear
18
19 and Circular Magnetic Dichroism of Fe_3O_4 . *J. Electron Spectrosc. Relat. Phenom.* **1997**, *86*,
20
21 107–113.
22

23
24
25 (48) Moyer, J. A.; Vaz, C. A. F.; Arena, D. A.; Kumah, D.; Negusse, E.; Henrich, V. E.
26
27 Magnetic Structure of Fe-Doped CoFe_2O_4 Probed by X-Ray Magnetic Spectroscopies. *Phys.*
28
29 *Rev. B* **2011**, *84*, 054447–054447 – 10.
30

31
32
33 (49) Kim, C. H.; Myung, Y.; Cho, Y. J.; Kim, H. S.; Park, S.-H.; Park, J.; Kim, J.-Y.; Kim, B.
34
35 Electronic Structure of Vertically Aligned Mn-Doped CoFe_2O_4 Nanowires and Their Application
36
37 as Humidity Sensors and Photodetectors. *J. Phys. Chem. C* **2009**, *113*, 7085–7090.
38

39
40
41 (50) Hocheplied, J. F.; Saintavit, P.; Pileni, M. P. X-Ray Absorption Spectra and X-Ray
42
43 Magnetic Circular Dichroism Studies at Fe and Co L_{2,3} Edges of Mixed Cobalt–zinc Ferrite
44
45 Nanoparticles: Cationic Repartition, Magnetic Structure and Hysteresis Cycles. *J. Magn. Magn.*
46
47 *Mater.* **2001**, *231*, 315–322.
48

49
50
51 (51) Byrne, J. M.; Coker, V. S.; Moise, S.; Wincott, P. L.; Vaughan, D. J.; Tuna, F.; Arenholz,
52
53 E.; van der Laan, G.; Patrick, R. A. D.; Lloyd, J. R.; *et al.* Controlled Cobalt Doping in Biogenic
54
55 Magnetite Nanoparticles. *J. R. Soc. Interface* **2013**, *10*:20130134.
56
57
58
59
60

1
2
3 (52) Sherman, D. M. Electronic Structures of iron(III) and manganese(IV) (hydr)oxide
4 Minerals: Thermodynamics of Photochemical Reductive Dissolution in Aquatic Environments.
5
6 *Geochim. Cosmochim. Acta* **2005**, *69*, 3249–3255.
7
8

9
10
11 (53) Groot, F. M. F. de; Abbate, M.; Elp, J. van; Sawatzky, G. A.; Ma, Y. J.; Chen, C. T.;
12 Sette, F. Oxygen 1s and Cobalt 2p X-Ray Absorption of Cobalt Oxides. *J. Phys. Condens.*
13 *Matter* **1993**, *5*, 2277–2288.
14
15
16

17
18
19 (54) Cao, C.-Y.; Qu, J.; Yan, W.-S.; Zhu, J.-F.; Wu, Z.-Y.; Song, W.-G. Low-Cost Synthesis
20 of Flowerlike A-Fe₂O₃ Nanostructures for Heavy Metal Ion Removal: Adsorption Property and
21 Mechanism. *Langmuir* **2012**, *28*, 4573–4579.
22
23
24
25

26
27 (55) Moussy, J.-B. From Epitaxial Growth of Ferrite Thin Films to Spin-Polarized Tunnelling.
28 *J. Phys. Appl. Phys.* **2013**, *46*, 143001-27.
29
30
31

32 (56) Hassnain Jaffari, G.; Ceylan, A.; Holt P Bui; Thomas P Beebe Jr; Ozcan, S.; S Ismat
33 Shah. *Journal of Physics: Condensed Matter*. **2012**, *24*, 336004-9.
34
35
36

37
38 (57) Li, M.; Mao, Y.; Yang, H.; Li, W.; Wang, C.; Liu, P.; Tog, Y. *New J. Chemistry*. *37*,
39 3116–3120.
40
41

42
43 (58) Zhou, Z.; Zhang, Y.; Wang, Z.; Wei, W.; Tang, W.; Shi, J.; Xiong, R. Electronic
44 Structure Studies of the Spinel CoFe₂O₄ by X-Ray Photoelectron Spectroscopy. *Appl. Surf. Sci.*
45 **2008**, *254*, 6972–6975.
46
47
48

49
50
51 (59) Jiménez, V. M.; Fernández, A.; Espinós, J. P.; González-Elipe, A. R. The State of the
52 Oxygen at the Surface of Polycrystalline Cobalt Oxide. *J. Electron Spectrosc. Relat. Phenom.*
53 **1995**, *71*, 61–71.
54
55
56
57
58
59
60

1
2
3 (60) Dupin, J.-C.; Gonbeau, D.; Vinatier, P.; Levasseur, A. Systematic XPS Studies of Metal
4 Oxides, Hydroxides and Peroxides. *Phys. Chem. Chem. Phys.* **2000**, *2*, 1319–1324.
5
6

7
8
9 (61) Wulser, K. W.; Langell, M. A. Carboxylic Acid Adsorption on NiO(100) Characterized
10 by X-Ray Photoelectron and High Resolution Electron Energy Loss Spectroscopies. *Catal. Lett.*
11 **1992**, *15*, 39–50.
12
13

14
15
16 (62) Cano, E.; Torres, C. L.; Bastidas, J. M. An XPS Study of Copper Corrosion Originated
17 by Formic Acid Vapour at 40% and 80% Relative Humidity. *Mater. Corros.* **2001**, *52*, 667–676.
18
19

20
21
22 (63) Cossaro, A.; Puppini, M.; Cvetko, D.; Kladnik, G.; Verdini, A.; Coreno, M.; de Simone,
23 M.; Floreano, L.; Morgante, A. Tailoring SAM-on-SAM Formation. *J. Phys. Chem. Lett.* **2011**,
24 *2*, 3124–3129.
25
26

27
28
29 (64) Wu, N.; Fu, L.; Su, M.; Aslam, M.; Wong, K. C.; Dravid, V. P. Interaction of Fatty Acid
30 Monolayers with Cobalt Nanoparticles. *Nano Lett.* **2004**, *4*, 383–386.
31
32

33
34
35 (65) Chen, C. T.; Idzerda, Y. U.; Lin, H.-J.; Smith, N. V.; Meigs, G.; Chaban, E.; Ho, G. H.;
36 Pellegrin, E.; Sette, F. Experimental Confirmation of the X-Ray Magnetic Circular Dichroism
37 Sum Rules for Iron and Cobalt. *Phys. Rev. Lett.* **1995**, *75*, 152–155.
38
39

40
41
42 (66) Thole, B. T.; Carra, P.; Sette, F.; van der Laan, G. X-Ray Circular Dichroism as a Probe
43 of Orbital Magnetization. *Phys. Rev. Lett.* **1992**, *68*, 1943–1946.
44
45

46
47
48 (67) Carra, P.; Thole, B. T.; Altarelli, M.; Wang, X. X-Ray Circular Dichroism and Local
49 Magnetic Fields. *Phys. Rev. Lett.* **1993**, *70*, 694–697.
50
51

52
53
54 (68) Cai, Y. P.; Chesnel, K.; Trevino, M.; Westover, A.; Harrison, R. G.; Hancock, J. M.;
55 Turley, S.; Scherz, A.; Reid, A.; Wu, B.; *et al.* Orbital and Spin Moments of 5 to 11 Nm Fe₃O₄
56
57
58
59
60

1
2
3 Nanoparticles Measured via X-Ray Magnetic Circular Dichroism. *J. Appl. Phys.* **2014**, *115*,
4 17B537-3.
5
6

7
8
9 (69) Rosensweig, R. E. Heating Magnetic Fluid with Alternating Magnetic Field. *J. Magn.*
10 *Magn. Mater.* **2002**, *252*, 370–374.
11
12

13
14 (70) Fortin, J.-P.; Wilhelm, C.; Servais, J.; Ménager, C.; Bacri, J.-C.; Gazeau, F. Size-Sorted
15 Anionic Iron Oxide Nanomagnets as Colloidal Mediators for Magnetic Hyperthermia. *J. Am.*
16 *Chem. Soc.* **2007**, *129*, 2628–2635.
17
18

19
20 (71) Martinez-Boubeta, C.; Simeonidis, K.; Makridis, A.; Angelakeris, M.; Iglesias, O.;
21 Guardia, P.; Cabot, A.; Yedra, L.; Estradé, S.; Peiró, F.; *et al.* Learning from Nature to Improve
22 the Heat Generation of Iron-Oxide Nanoparticles for Magnetic Hyperthermia Applications. *Sci.*
23 *Rep.* **2013**, *3*, 1652-8.
24
25

26
27 (72) Burrows, F.; Parker, C.; Evans, R. F. L.; Hancock, Y.; Hovorka, O.; Chantrell, R. W.
28 Energy Losses in Interacting Fine-Particle Magnetic Composites. *J. Phys. Appl. Phys.* **2010**, *43*,
29 474010-10.
30
31

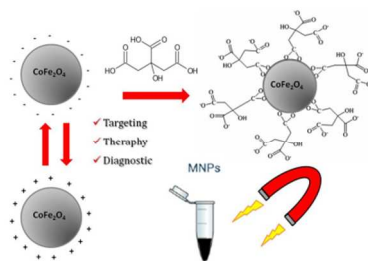
32
33 (73) Atak, K.; Bokarev, S. I.; Gotz, M.; Golnak, R.; Lange, K. M.; Engel, N.; Dantz, M.;
34 Suljoti, E.; Kühn, O.; Aziz, E. F. Nature of the Chemical Bond of Aqueous Fe²⁺ Probed by Soft
35 X-Ray Spectroscopies and Ab Initio Calculations. *J. Phys. Chem. B* **2013**, *117*, 12613–12618.
36
37

38
39 (74) Gotz, M. D.; Soldatov, M. A.; Lange, K. M.; Engel, N.; Golnak, R.; Könnecke, R.; Atak,
40 K.; Eberhardt, W.; Aziz, E. F. Probing Coster–Kronig Transitions in Aqueous Fe²⁺ Solution
41 Using Inverse Partial and Partial Fluorescence Yield at the L-Edge. *J. Phys. Chem. Lett.* **2012**, *3*,
42 1619–1623.
43
44
45
46
47
48
49
50
51
52
53
54
55
56
57
58
59
60

(75) Seidel, R.; Ghadimi, S.; Lange, K. M.; Bonhommeau, S.; Soldatov, M. A.; Golnak, R.; Kothe, A.; Könnecke, R.; Soldatov, A.; Thürmer, S.; *et al.* Origin of Dark-Channel X-Ray Fluorescence from Transition-Metal Ions in Water. *J. Am. Chem. Soc.* **2012**, *134*, 1600–1605.

(76) Blum, M.; Weinhardt, L.; Fuchs, O.; Bär, M.; Zhang, Y.; Weigand, M.; Krause, S.; Pookpanratana, S.; Hofmann, T.; Yang, W.; *et al.* Solid and Liquid Spectroscopic Analysis (SALSA)—a Soft X-Ray Spectroscopy Endstation with a Novel Flow-through Liquid Cell. *Rev. Sci. Instrum.* **2009**, *80*, 123102.

TOC



Three types of CoFe₂O₄ NPs differently stabilized in aqueous solution were prepared for biomedical applications. A detailed spectroscopic study has shown that the surface modification does not affect the electronic and magnetic properties of the NPs.